Numerical Evolution of Plane Gravitational Waves

Jonathan Hakata
19H7984

Department of Mathematics and Applied Mathematics

Faculty of Science

Rhodes University

Submitted in full satisfaction of the requirements for the
Degree of Master of Science
in Applied Mathematics

Supervisor Dr. Chris Stevens
Second Supervisor Prof. Denis Pollney

March 2021

Declaration

I hereby declare that this thesis is all my own work, except as indicated in the text:

Signature: 

Date: 18 / 08 / 21

Acknowledgements

I would like to relay my heartfelt gratitude to The Henderson Scholarship, administered at Rhodes University's Postgraduate Funding Office, for the financial support which enabled me pursue my studies over the past two years. I wish to extend my special thanks to my supervisor Dr. Chris Stevens[1] for all the in-depth knowledge passed and encouragement he gave me. His insight and knowledge into the subject matter steered me through this research and without him this Masters would not have been achievable. Special mention goes to Prof. Denis Pollney[2] for co-supervising me through this research work.

My grateful thanks are also extended to my family, to lecturers and college mates in the Mathematics Department here at Rhodes University for the moral support and interesting discussions inclined to the course of my studies.

[1]Currently a Mathematics lecturer at University of Otago, NZ
[2]Head of the Mathematics and Applied Mathematics Department at Rhodes University, SA

Abstract

Unlike electromagnetic waves, gravitational waves self interact. This interaction is non-linear and can have very interesting properties which effect the curvature of space-time. A gravitational plane wave collider, implemented in the `Python` package COFFEE [20] that been developed in recent years by the Otago relativity group and implements the method of lines, can be reliably used to study this self-interaction. This was shown to work well numerically as profounded by Frauendiener, Stevens and Whale in 2014 [24]. For this reason, COFFEE will be used to study these gravitational wave propagations and subsequently collisions.

The Einstein field equations are formulated as a well-posed initial boundary value problem (IBVP) in the Friedrich-Nagy gauge [26] and due to the large class of boundary conditions admitted by this framework, a variety of investigations into the propagation of plane gravitational waves could be carried out.

This study focuses on the propagation of plane gravitational waves in the de Sitter (dS) space-time, which is the maximally symmetric solution of the Einstein's vacuum field equations with a positive cosmological constant λ. There is substantial cosmological evidence that our universe is asymptotically de Sitter, yet no work, analytical nor numerical, has been done on gravitational plane waves propagating on such a space-time, mainly due to the increased complexity from the non-vanishing λ.

Firstly, it is found analytically that with an arbitrary cosmological constant λ and a non-vanishing energy momentum tensor, the constraints will propagate. This means that we still have a wellposed IBVP, which is nontrivial since the Friedrich-Nagy gauge has only been shown to lead to a wellposed IBVP without matter [26]. Using this system, we consider one ingoing wave propagating on said space-time in vacuum. The area of the ingoing wave profile is varied and inferences are made about the different phenomena that arise in the curvature of

space-time during the evolution. It is found that there exists a critical value of the wave's area, a_c, whereby taking the area below this value the system asymptotes to its initial state, and above the system diverges, indicating the presence of a singularity. Furthermore, we define an expansion parameter H to measure how the gravitational waves influence the accelerated expansion, generalising (numerically) results of Tsamis and Woodard [48].

Table of Contents

List of Figures

Chapter 1

Introduction

The **Theory** of General Relativity, a postulate by Albert Einstein in November 1915 [14], explains that what we perceive as the force of gravity in fact arises from the curvature of space and time. He put forward the well known non-linear Einstein field equations (EFEs) (see Appendix A.9) which describe the gravitational field. The equations match the curvature of local space-time to the local energy and momentum within that space-time. These equations have since been shown to have wave solutions [28]. According to this theory, perturbations of space-time curvature, generated by accelerated masses, are known as gravitational waves and these propagate at the speed of light, just like electromagnetic waves.

Traditional means such as optical telescopes or radio telescopes have been and are still being used to observe and understand our universe but are limited due to scattering, absorption and long distances travelled by the electromagnetic waves they detect. On the other hand gravitational waves can penetrate regions of space that electromagnetic waves cannot due to their weak interactions with matter. They do so while carrying undistorted information about their sources. Phenomena like merging neutron stars, colliding black holes and exploding stars which was utterly invisible to electromagnetic astronomers have become *seeable* by detecting and analysing gravitational waves they produce. This has created a new window in multi-messenger astronomy with which scientists can use to see all the way back even to the origin of the cosmos itself. Thus gravitational wave astronomy gives new insights into the working of the universe.

Due to the faintness and weakness of the gravitational waves, though being detectable, Einstein wondered if they could ever be discovered and be useful in science. However, almost 100 years after his postulate, on 14 September 2015, gravita-

tional waves were finally directly detected [50]. The existence of such waves has further been proven with other several recent detections by the Laser Interferometer Gravitational wave Observatory (LIGO) and VIRGO collaboration [1, 2]. Unlike electromagnetic waves which superpose rather than self interact when they collide, gravitational waves interact non-linearly [28]. Though this phenomenon is very weak so much that it is very hard to detect, its study is intriguing as we strive to understand our universe in greater depth.

As a first attempt at studying this non-linear self-interaction, one must consider some sort of simplifying assumptions. Taking a vanishing cosmological constant and plane symmetry in vacuum is what people have been drawn toward. Spherical symmetry is neglected as by Birkhoff's theorem, this precludes the existence of gravitational waves. As a final simplification, one considers only one wave.

Thus, consider the evolution of a **plane** gravitational **wave** in Minkowski space. Griffiths in [28] highlights that the widely known class of plane-fronted gravitational waves having parallel rays are the *pp*-waves first introduced by by Jürgen Ehlers and Wolfgang Kundt in 1962, see [23]. The term *pp* being an acronym for *parallel propagation*. Their definition is based upon their property of admitting a covariantly constant null vector field identified by the tetrad vector l^a, that is the covariant derivative of l^a must vanish. The field components for *pp*-waves are the same at all the points of the wave surfaces and for this very reason they are plane symmetric. Using the null coordinate u, the line element for a plane wave can then be defined as

$$\mathrm{d}s^2 = 2\mathrm{d}u\mathrm{d}r + (h_{11}X^2 + 2h_{12}XY + h_{22}Y^2)\mathrm{d}u^2 - \mathrm{d}X^2 - \mathrm{d}Y^2 \tag{1.1}$$

where h_{ij} are functions of u alone and X and Y are the space-like coordinates spanning the wave surfaces.

Another interesting class of gravitational waves admitting these simplifying assumptions are the sandwich waves. Podolskỳ and Veselỳ in 1998 explored examples of sandwich gravitational waves in [42]. They found out that sandwich gravitational waves can be constructed from the homogenous pp-solution in the case where du is non-zero on some $u \in [u_1, u_2]$. For this case the spacetime can be split into three distinct regions similar to the work put forward by Khan and Penrose in [31] which is the first exact solution for the case of colliding plane

impulsive gravitational waves. The regions $u < u_1$, $u_1 < u < u_2$ and $u > u_2$ are flat, curved and flat respectively. In order to describe this class of waves, the line element (1.1) above can also be used.

Earlier work by Bondi et al in 1959 [12] as well as Bondi and Pirani in 1989 [11] further analysed the focusing property of plane waves explaining it in terms of caustics. They probed the action of sandwich plane gravitational waves onto a collection of test particles that are initially at rest in a Minkowski spacetime. The particles were strung in a fixed direction determined by the polarisation of the wave. They observed that for the case of waves having a constant linear polaristion, all the particles collided after a certain known time irrespective of their initial positions and such is the focusing power of gravitational waves. Penrose in 1965 (see [40]) had also made a similar finding which was remarkable by that time. In the same article [11], geometrical properties of plane gravitational waves were explored. They found out that an observer, after passing through the front of such a wave, will after a predetermined time have seen the entire spatial volume lying in a space-like half-hyperplane in front of the wave.

There are also a class of space-times that describe the collision of plane-fronted gravitational waves with colinear polarisation. This was put forward by Khan and Penrose in 1971 [31] where the two waves had delta-function wave profiles (called impulsive waves.) This solution was generalised later by Nutku and Halil to include arbitrary polarisations [36]. They found that the space-time was split into four regions: The initial region between the waves (Minkowski space-time), two regions containing one wave each and the interaction region. Suprisingly, the interaction region contained an unavoidable future space-like curvature singularity. This was postulated to be an artifact of the plane symmetry.

With the large study of plane gravitational waves in Minkowski space, the question arises: What happens if we make the cosmological constant non-zero? The simplest space-times with positive and negative cosmological constant are the de Sitter and anti-de Sitter space-times respectively. In 1999 Podolský and Bičák in [9] carried out an analytical investigation into gravitational waves in de Sitter and anti-de Sitter backgrounds. They analysed properties of non-twisting type N solutions of the vacuum Einstein field equations. They found that for a non-vanishing cosmological constant there exist two cases to consider i.e (i) the Kundt

class of non-expanding gravitational waves and (ii) the Robinson-Trautman class of expanding gravitational waves. Within the same year, they put forward work on the physical properties of these type N solutions also referred to as transverse gravitational waves. There has been no investigations done into plane gravitational waves propagating in de Sitter space-time.

There is enough undeniable evidence in literature that our universe is expanding at an accelerated rate. The expansion of the universe is merely an increase in length of path between two gravitationally unbound parts of the universe over time [37, 45]. Early work done by Edwin Hubble in 1929 [30] suggested beyond doubt that the universe was expanding. In his work he measured the velocities of a number of nearby galaxies and discovered that they were moving away from us and this has been verified by observing galaxies using better equipment [45]. This accelerated expansion can be realised mathematically by including a positive cosmological constant into the Einstein equations. De Sitter space-time is a simple example of an expanding universe where the expansion is accelerating at a constant rate.

Recently Woodard and Tsamsis in [47, 48] carried out an investigation into the effects of gravitational waves on the expansion rate of the de Sitter space-time. Once clarifying what they mean by expansion rate of the perturbed space-time, they showed that on an initial timeslice, gravitational waves do indeed affect the expansion rate due to the modified extrinsic curvature. They defined this expansion rate $H(t, \mathbf{x})$ as

$$H(t, \mathbf{x}) = \frac{1}{3} D^{\mu} u_{\mu}(t, \mathbf{x}) \tag{1.2}$$

in terms of a covariant derivative D^{μ} of a time-like four velocity vector field u_{μ}.

In order to investigate the propagation of plane gravitational waves in the de Sitter space-time, we turn to numerical solutions of the EFEs. To accomplish this, it is useful to formulate them as an IBVP as demonstrated by Fraundiener et al in [24], who consider the numerical evolution of plane gravitational waves in Minkowski space-time, implementing the system in the Python package COFFEE [20]. This formulation involves the introduction of artificial timelike boundaries to reduce the physically-infinite system to a finite one. They highlight that one will be left with the question as to which boundary conditions guarantees the existence of

a unique solution to the Einstein's equations which admits the given values on the initial data hypersurface and boundary. The set up put forward by Friedrich and Nagy in [26] is then utilised which implements the Einstein equations in the Newman-Penrose formalism [34] and the resulting IBVP and was analytically proved to be wellposed in vacuum with an arbitrary cosmological constant.

In this work we seek to analyse numerically the de Sitter spacetime perturbed by plane gravitational waves. This is achieved by imposing an initial boundary value problem to the EFEs, generalising [24] by including a cosmological constant. We seek to investigate the influence of the wave profiles on the resulting space-time, in particular the curvature and expansion rate. A critical phenomenon is discovered and analysed in detail.

1.1 Objectives

1.1.1 General objective

To numerically evolve a single plane gravitational wave on a de Sitter space-time in the Friedrich-Nagy gauge using the aforementioned COFFEE and characterise the resulting space-time.

1.1.2 Specific objectives

1. Experiment with different wave profiles using the numerical framework developed and tested in [24] to find interesting cases of the evolved gravitational waves by modifying their area and amplitude.
2. Analyse the perturbed space-time by looking at:
    - The Kretschmann scalar, a scalar curvature invariant, to see whether any physical curvature singularities occur.
    - A self-defined expansion parameter, to measure how introducing a gravitational wave affects the accelerated expansion of the space-time.

1.2 Description of the work

Having drawn the road map for the entire study in this first chapter, the following section contains literature reviews of previous researches and their significance to the context under study. Derivations of the field equations and other essential equations in the Friedrich - Nagy gauge with a cosmological constant are presented in Chapter 3. This is then followed by a discussion regarding the numerical tools, setup as well as implementations executed to achieve the research objectives. Chapter 5 is devoted to an analysis, presentation and evaluation of findings and their applications. Reflections, recommendations for future work and an overall summary of this research are presented in Chapter 6. Additional material deemed necessary to follow this research are then provided in the appendices.

Part I

Plane Gravitational Waves

Chapter 2

Literature Review

2.1 The Newman-Penrose Formalism

In 1962, ideas from Penrose's spinors [38] and Newman's tetrad approach were brought together to formulate the well known Newman-Penrose (N-P) formalism [34]. This approach has proven very useful for many applications in general relativity as it allows for simplification of many theorems in the study of gravitational radiation and for the search of exact solutions [49]. Griffiths further points out that the N-P formalism facilitates the geometrical analysis of the colliding plane wave problem [28]. The main ingredients of this technique are the spin coefficients and its usefulness relies on the fact that the end equations are first order and so can be grouped into linear equations. In addition, all the equations become complex thereby reducing the total number by half and this allows the reduced number of equations to be written explicitly without the use of index and summation conventions. For these same reasons the Friedrich-Nagy (F-N) gauge which shall be employed in this research was formulated using the N-P formalism [39] and it makes sense to derive our field equations using the same technique.

In this section, we review and closely follow the derivations put forward by Griffiths in [28]. In 1962 Newman and Penrose put forward the most convenient approach of representing Einstein's equations well known as the Newman-Penrose formalism [34]. This involves the introduction of a tetrad system of null vectors

$$(l^{\mu}, n^{\mu}, m^{\mu}, \bar{m}^{\mu}) \tag{2.1}$$

where l^μ and n^μ are real null vectors and m^μ is a complex null vector along with its conjugate $\bar{m}^\mu$. All their inner products are zero except

$$l_\mu n^\mu = 1, \qquad m_\mu \bar{m}^\mu = -1. \tag{2.2}$$

It can then be shown (see Appendix) that in terms of the null tetrad basis, the metric tensor becomes

$$g_{\mu\nu} = l_\mu n_\nu + n_\mu l_\nu - m_\mu \bar{m}_\nu - \bar{m}_\mu m_\nu. \tag{2.3}$$

Having defined this basis, the Ricci and Weyl tensor components can now be given.

2.1.1 The Ricci Tensor

The ten independent components of the Ricci tensor ($R_{\mu\nu}$) can now be divided into a component λ (in vacuum $\lambda = \frac{1}{6}\lambda$ where λ is the cosmological constant) which represents the curvature scalar and nine independent components of a Hermitian 3×3 matrix Φ_{AB}, which represents the trace-free part of the Ricci tensor satisfying $\Phi_{AB} = \Phi_{BA}$. Indices AB can take values $0, 1, 2$ [28]. These components can be defined as

$$\begin{aligned}
\Phi_{00} &= -\frac{1}{2}R_{\mu\nu}l^\mu l^\nu & \Phi_{11} &= -\tfrac{1}{4}R_{\mu\nu}(l^\mu n^\nu + m^\mu \bar{m}^\nu) \\
\Phi_{10} = \Phi_{01} &= -\frac{1}{2}R_{\mu\nu}l^\mu m^\nu & \Phi_{21} = \Phi_{12} &= -\tfrac{1}{2}R_{\mu\nu}n^\mu m^\nu \\
\Phi_{20} = \Phi_{02} &= -\frac{1}{2}R_{\mu\nu}m^\mu m^\nu & \Phi_{22} &= -\tfrac{1}{2}R_{\mu\nu}n^\mu n^\nu \\
\lambda &= \frac{1}{24}R.
\end{aligned}$$

2.1.2 The Weyl Tensor

The free gravitational field is then represented by the ten components of the Weyl tensor (Ψ_i) conveniently expressed as the five complex scalars

$$\begin{aligned}
\Psi_0 &= -C_{\kappa\lambda\mu\nu}l^\kappa m^\lambda l^\mu m^\nu & \Psi_3 &= -C_{\kappa\lambda\mu\nu}n^\kappa l^\lambda n^\mu \bar{m}^\nu \\
\Psi_1 &= -C_{\kappa\lambda\mu\nu}l^\kappa n^\lambda l^\mu m^\nu & \Psi_4 &= -C_{\kappa\lambda\mu\nu}n^\kappa \bar{m}^\lambda n^\mu \bar{m}^\nu. \\
\Psi_2 &= -C_{\kappa\lambda\mu\nu}l^\kappa m^\lambda \bar{m}^\mu n^\nu
\end{aligned}$$

Interpretations for these Weyl tensor components are as follows:

- Ψ_0 represents a transverse wave component in the n^μ direction.
- Ψ_1 represents a longitudinal wave component in the n^μ direction.
- Ψ_2 represents a coulomb component.
- Ψ_3 represents a longitudinal wave component in the l^μ direction.
- Ψ_4 represents a transverse wave component in the l^μ direction.

Such an interpretation is important when analysing gravitational wave propagations and consequently interactions.

2.1.3 The Spin Coefficients

Spin coefficients are the main feature of the Newman-Penrose formalism. These are obtained from complex linear combinations of the Ricci rotation coefficients associated with the null tetrad mentioned earlier. Although we are following the outline as given by Griffiths as mentioned earlier, we adopt conventions by Penrose and Rindler in [39].The spin coefficients are defined as

$$\begin{aligned}
\kappa &= l_\mu \nabla_\nu m^\mu l^\nu & \kappa' &= n_\mu \nabla_\nu \bar{m}^\mu n^\nu \\
\rho &= l_\mu \nabla_\nu m^\mu \bar{m}^\nu & \rho' &= n_\mu \nabla_\nu \bar{m}^\mu m^\nu \\
\sigma &= l_\mu \nabla_\nu m^\mu m^\nu & \sigma' &= n_\mu \nabla_\nu \bar{m}^\mu \bar{m}^\nu \\
\tau &= l_\mu \nabla_\nu m^\mu n^\nu & \tau' &= n_\mu \nabla_\nu \bar{m}^\mu l^\nu \\
\epsilon &= \tfrac{1}{2}(l_\mu \nabla_\nu n^\mu l^\nu - m_\mu \nabla_\nu \bar{m}^\mu l^\nu) & \beta &= \tfrac{1}{2}(l_\mu \nabla_\nu n^\mu m^\nu - m_\mu \nabla_\nu \bar{m}^\mu m^\nu) \\
\alpha &= \tfrac{1}{2}(l_\mu \nabla_\nu n^\mu \bar{m}^\nu - m_\mu \nabla_\nu \bar{m}^\mu \bar{m}^\nu) & \gamma &= \tfrac{1}{2}(l_\mu \nabla_\nu n^\mu n^\nu - m_\mu \nabla_\nu \bar{m}^\mu n^\nu).
\end{aligned} \tag{2.4}$$

It will be more convenient to describe and analyse the geometric properties of solutions in terms of these spin coefficients later in this study.

The commutator relations between the directional derivatives (D, D', δ and δ') defined in section (3.7) below that act on scalars are given as

$$\begin{aligned}
D'D - DD' &= (\gamma + \bar{\gamma})D - (\gamma' + \bar{\gamma}')D' - (\tau - \bar{\tau}')\delta' + (\tau' - \bar{\tau})\delta \\
\delta D - D\delta &= (\beta + \bar{\alpha} + \bar{\tau}')D + \kappa D' - \sigma\delta' - (\epsilon + \bar{\gamma}' + \bar{\rho})\delta \\
\delta D' - D'\delta &= \bar{\kappa}'D + (\tau + \bar{\beta}' + \alpha')D' - \bar{\sigma}'\delta' - (\bar{\epsilon}' + \gamma + \rho')\delta \\
\delta'\delta - \delta\delta' &= (\rho' - \bar{\rho}')D - (\rho - \bar{\rho})D' - (\alpha' + \bar{\alpha})\delta' + (\alpha + \bar{\alpha}')\delta.
\end{aligned} \tag{2.5}$$

The next set of useful equations in this formalism are the curvature equations.

These are merely derivatives of spin coefficients found by applying the relations above on spin coefficients and they are given in general by

$$
\begin{aligned}
D\rho - \delta'\kappa &= \rho^2 + \sigma\bar{\sigma} - \bar{\kappa}\tau - \kappa(\tau' + 2\alpha + \bar{\beta} - \beta') + \rho(\epsilon + \bar{\epsilon}) + \Phi_{00},\\
D\sigma - \delta\kappa &= \sigma(\rho + \bar{\rho} + \bar{\gamma}' - \gamma' + 2\epsilon) - \kappa(\tau + \bar{\tau}' + \alpha - \alpha' + 2\beta) + \Psi_0,\\
D\tau - D'\kappa &= \rho(\tau - \bar{\tau}') + \sigma(\bar{\tau} - \tau') + \tau(\bar{\gamma}' + \epsilon) - \kappa(\bar{\gamma} + 2\gamma - \epsilon') + \Psi_1 + \Phi_{01},\\
\delta\rho - \delta'\sigma &= \tau(\rho - \bar{\rho}) + \kappa(\bar{\rho}' - \rho') + \rho(\bar{\alpha} + \beta) - \sigma(\bar{\alpha}' + 2\alpha - \beta') - \Psi_1 + \Phi_{01},\\
\delta\tau - D'\sigma &= -\rho'\sigma - \bar{\sigma}'\rho + \tau^2 + \kappa\bar{\kappa}' + \tau(\beta + \bar{\beta}') - \sigma(2\gamma - \epsilon' + \bar{\epsilon}') + \Phi_{02},\\
D'\rho - \delta'\tau &= \rho\bar{\rho}' + \sigma\sigma' - \tau\tau' - \kappa\kappa' + \rho(\gamma + \bar{\gamma}) - \tau(\alpha + \bar{\alpha}') - \Psi_2 - 2\lambda,\\
D'\beta - \delta\gamma &= \tau\rho' - \kappa'\sigma - \bar{\kappa}'\epsilon + \alpha\bar{\sigma}' + \beta(\rho' + \bar{\epsilon}' + \gamma) - \gamma(\bar{\beta}' + \alpha' + \tau) - \Phi_{12},\\
\delta'\epsilon - D\alpha &= \tau'\rho - \kappa\sigma' + \bar{\kappa}\gamma - \beta\bar{\sigma} - \alpha(\rho + \bar{\epsilon} + \gamma') + \epsilon(\bar{\beta} + \alpha + \tau') - \Phi_{10},\\
D\beta - \delta\epsilon &= \kappa(\rho' - \gamma) - \sigma(\tau' - \alpha) + \beta(\bar{\rho} + \bar{\gamma}') - \epsilon(\bar{\tau}' + \bar{\alpha}) + \Psi_1,\\
\delta'\gamma - D'\alpha &= \kappa'(\rho + \epsilon) - \sigma'(\tau + \beta) - \alpha(\bar{\rho}' + \bar{\gamma}) + \gamma(\bar{\tau} + \bar{\alpha}') + \gamma\beta' - \epsilon'\alpha + \Psi_3,
\end{aligned}
$$

$$
\begin{aligned}
D\gamma - D'\epsilon &= \kappa\kappa' - \tau\tau' - \beta(\tau' - \bar{\tau}) - \alpha(\bar{\tau}' - \tau) - \epsilon(\gamma + \bar{\gamma}) + \gamma(\gamma' + \bar{\gamma}')\\
&\quad + \Psi_2 + \Phi_{11} - \lambda,\\
\delta'\beta - \delta\alpha &= \rho\rho' - \sigma\sigma' - \alpha\bar{\alpha} + \beta\bar{\alpha}' + \alpha(\beta - \alpha') + \gamma(\bar{\rho} - \rho) + \epsilon(\rho' - \bar{\rho}')\\
&\quad + \Psi_2 - \Phi_{11} - \lambda. \qquad (2.6)
\end{aligned}
$$

The other twelve curvature equations in addition to the above are found by performing the priming operation on (2.6) [49].

The other essential part of the Newman-Penrose formalism is the set of equations known as the Bianchi identities [35]. These can be regarded as equations for the Weyl tensor components (Ψ_i), and as put forward by Penrose and Rindler in [39] they are given as

$$
\begin{aligned}
D\Psi_1 - \delta'\Psi_0 - D\Phi_{01} + \delta\Phi_{00} &= -\tau'\Psi_0 + 4\rho\Psi_1 - 3\kappa\Psi_2 + \bar{\tau}'\Phi_{00} \\
&\quad - 2\bar{\rho}\Phi_{01} - 2\sigma\Phi_{10} + 2\kappa\Phi_{11} + 2\bar{\kappa}\Phi_{02}, \\
D\Psi_2 - \delta'\Psi_1 - \delta\Phi_{01} + D'\Phi_{00} + 2D\lambda &= \sigma'\Psi_0 - 2\tau'\Psi_1 + 3\rho\Psi_2 - 2\kappa\Psi_3 + \bar{\rho}'\Phi_{00} \\
&\quad - 2\bar{\tau}\Phi_{01} - 2\tau\Phi_{10} + 2\rho\Phi_{11} + \bar{\sigma}\Psi_{02}, \\
D\Psi_3 - \delta'\Psi_2 - D\Phi_{21} + \delta\Phi_{20} - 2\delta'\lambda &= 2\sigma'\Psi_1 - 3\tau'\Psi_2 + 2\rho\Psi_3 - \kappa\Psi_4 - 2\rho'\Phi_{10} \\
&\quad + 2\tau'\Phi_{11} + \bar{\tau}'\Phi_{20} - 2\bar{\rho}\Phi_{21} + \bar{\kappa}\Phi_{22}, \\
D\Psi_4 - \delta'\Psi_3 - \delta'\Phi_{21} + D'\Phi_{20} &= 3\sigma'\Psi_2 - 4\tau'\Psi_3 + \rho\Psi_4 - 2\kappa'\Phi_{10} + 2\sigma'\Phi_{11} \\
&\quad + \bar{\rho}'\Phi_{20} - 2\bar{\tau}\Phi_{21} + \bar{\sigma}\Phi_{22}, \\
D\Phi_{11} + D'\Phi_{00} - \delta\Phi_{10} - \delta'\Phi_{01} + 3D\lambda &= (\rho' + \bar{\rho}')\Phi_{00} + 2(\rho + \bar{\rho})\Phi_{11} \\
&\quad - (\tau' + 2\bar{\tau})\Phi_{01} - (2\tau + \bar{\tau}')\Phi_{10} - \bar{\kappa}\Phi_{12} \\
&\quad - \kappa\Phi_{21} + \sigma\Phi_{20} + \bar{\sigma}\Phi_{02}, \\
D\Phi_{12} + D'\Phi_{01} - \delta\Phi_{11} - \delta'\Phi_{02} + 3\delta\lambda &= (\rho' + 2\bar{\rho}')\Phi_{01} + (2\rho + \bar{\rho})\Phi_{12} \\
&\quad - (\tau' + \bar{\tau})\Phi_{02} - 2(\tau + \bar{\tau}')\Phi_{11} - \bar{\kappa}'\Phi_{00} \\
&\quad - \kappa\Phi_{22} + \sigma\Phi_{21} + \bar{\sigma}'\Phi_{10}. \qquad (2.7)
\end{aligned}
$$

The other missing equations will be the primed versions of these. In the next chapter, equations (2.5), (2.6) and (2.7) will be reviewed to the case under study subject to some necessary simplifications in deriving the field equations in this formalism.

2.2 Plane gravitational waves in Minkowski spacetime

Hawking and Ellis in [29] define the Minkowski spacetime ($\mathcal{M}$) as the simplest empty spacetime in General Relativity, mathematically being the manifold $\mathbb{R}^4$ with a flat Lorentz metric η that can be expressed in the form

$$
\mathrm{d}s^2 = -(\mathrm{d}t)^2 + (\mathrm{d}x)^2 + (\mathrm{d}y)^2 + (\mathrm{d}z)^2
$$

for the natural coordinates (t, x, y, z) in $\mathbb{R}^4$.

Griffiths in [28] did put forward a discussion on a class of solutions to the EFEs

known as the *pp*-waves discovered earlier by Brinkmannn (1923). These plane fronted gravitational waves are known to admit a null vector field that is covariantly constant and so a tetrad vector l^μ can be identified with this field. From the properties defining l^μ that $l_{\mu;\nu} = 0$ it immediately follows that this vector field is tangent to a wave surface like Minkowski spacetime which is non-expanding and bearing neither shear nor twist null geodesic congruence. Owing to the congruence being expansion-free, such wave surfaces are said to be plane. For a null coordinate u such that $l_\mu = \frac{\partial u}{\partial x^\mu}$, the line element known to represent the *pp*-wave spacetime in the Kerr-Schild form is

$$\mathrm{d}s^2 = 2\mathrm{d}u\mathrm{d}r + H(u, X, Y)\mathrm{d}u^2 - \mathrm{d}X^2 - \mathrm{d}Y^2 \tag{2.8}$$

with space-like coordinates X and Y spanning the wave surfaces and H being a smooth metric function. For these metrics, Griffiths then points out that the only curvature components which are non-zero are

$$\begin{aligned} \Phi_{22} &= \frac{1}{4}(H_{,XX} + H_{,YY}) \\ \Psi_4 &= \frac{1}{4}(H_{,XX} - H_{,YY} + 2iH_{,XY}). \end{aligned} \tag{2.9}$$

The consequence of this is that the line element Eqn.(2.8) satisfies the Einstein's vacuum equations if and only if $H_{,XX} + H_{,YY} = 0$ that is if the Ricci tensor Φ_{ij} components are zero [51, 41]. Moreso, a *pp*-gravitational plane wave is one with the same field components at every point of the wave surfaces and so is said to exhibit plane symmetry. For such a wave with constant linear polarization the line element is then

$$\mathrm{d}s^2 = 2\mathrm{d}u\mathrm{d}r + h_{11}(u)(X^2 - Y^2)\mathrm{d}u^2 - \mathrm{d}X^2 - \mathrm{d}Y^2 \tag{2.10}$$

with $\Psi_4 = h_{11}(u)$ having removed H terms linear in X and Y by coordinate transformation.

Impulsive plane gravitational waves propagating in Minkowski spacetime have been looked into in the past. Podolskỳ et al in [43] defines them as mere theoretical models of gravitational bursts, which are short but violent, first introduced by Penrose in the late 1960s (see [41] p.82). These can be constructed on a Minkowski background using the 'cut and paste' approach put forward by Penrose in [41]. Griffiths in [28] puts forward a detailed discussion on these and for a

null coordinate u the Brinkmann-Peres-Takeno line element can used to describe one such wave as

$$\mathrm{d}s^2 = 2\mathrm{d}u\mathrm{d}r + \delta(u)(X^2 - Y^2)\mathrm{d}u^2 - \mathrm{d}X^2 - \mathrm{d}Y^2 \tag{2.11}$$

where $\delta(u)$, the Dirac delta function, being a component of the impulsive wave.

In 1971, Khan and Penrose [31] obtained the first exact solution for colliding plane impulsive gravitational waves in a flat region of Minkowski background. It was remarkably noted from this pioneering work that the spacetime before the collision was flat and after the collision was not only curved, but developed a future curvature singularity. Metrics describing approaching impulsive plane gravitational waves are well known [28] and one such metric is

$$g = \frac{2T^3 dU dV}{RW(PQ+RW)^2} - T^2\left(\frac{R+Q}{R-Q}\right)\left(\frac{W+P}{W-P}\right)dX^2 - T^2\left(\frac{R-Q}{R+Q}\right)\left(\frac{W-P}{W+P}\right)dY^2 \tag{2.12}$$

where

$$P = U\Theta(U), \quad Q = V\Theta(V), \quad R = (1-P^2)^{1/2}, \quad w = (1-Q^2)^{1/2},$$
$$T = (1-P^2-Q^2)^{1/2} \tag{2.13}$$

in which Θ is the Heaviside step function. Using a suitable symbolic manipulation, the same line element was transformed and together with the gravitational wave components Ψ_4 and Ψ_0, the initial situation of two approaching waves was defined. The form of the metric (2.12) suggests that the spacetime divides into four different regions in a natural way using the signs of U and V as illustrated below.

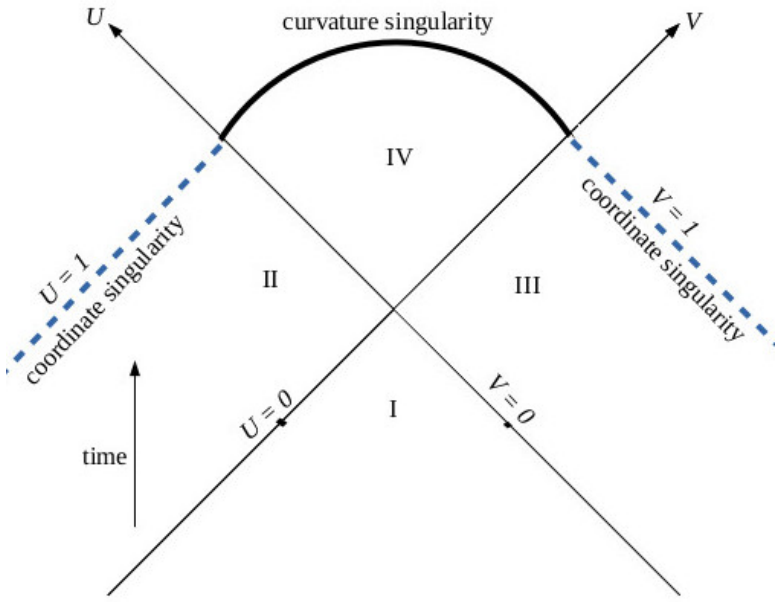

Figure 2.1: The singularity structure of the Khan-Penrose solution.

Region I ($U \leq 0$, $V \leq 0$) represents the flat background, Region II ($U \geq 0$, $V \leq 0$) and III ($U \leq 0$, $V \geq 0$) contain the two approaching waves. Region IV ($U > 0$, $V > 0$) is the interaction region following the collision, which is not flat. Khan and Penrose found that the line element in this region was a unique solution to the Einstein's vacuum equations subject to appropriate boundary conditions set on the two null surfaces $V = 0$, $U \geq 0$ and $U = 0$, $V \geq 0$. The equation for this line element is given in the Appendix. It was also noted that metrics for regions II and III are singular on the null hypersurface $U = 1$ and $V = 1$ respectively. They regarded these as coordinate singularities since they could be removed by suitable coordinate transformations.

Tremendous work for the case of gravitational waves propagating in Minkowski spacetime has been done in recent years and one such investigation was done by Wulandari and Triyanta in [17]. They found out that the passing of gravitational waves which carry along the fluctuation effect causes ripples in spacetime making each of the rest particles present feel a tidal acceleration.

Clearly from the available literature there is no doubt that most exact solutions for the Einstein vacuum equations are for impulsive plane gravitational waves on flat backgrounds. These have been heavily studied because analytical solutions can be found for them. For these same reasons this work seeks to fill up the

gap in literature by considering the case of plane gravitational waves evolved numerically on a de Sitter background followed by an analysis of the perturbed spacetime. This will involve comparing and contrasting the findings with what could be achieved in Minkowski spacetime.

2.3 Plane gravitational waves in de Sitter spacetime

Hawking and Ellis in [29] define the de Sitter spacetime as a space of constant curvature for $\lambda > 0$ having a topology $R^1 \times S^3$. It is easily visualised as a hyperboloid

$$-v^2 + w^2 + x^2 + y^2 + z^2 = \alpha^2 \tag{2.14}$$

and in a flat R^5 space has metric

$$-\mathrm{d}v^2 + \mathrm{d}w^2 + \mathrm{d}x^2 + \mathrm{d}y^2 + \mathrm{d}z^2 = \mathrm{d}s^2. \tag{2.15}$$

In flat slicing which is implemented in this work, for coordinates (t, x, y, z) on $\mathbb{R}^4$, it can be partly covered by the line element

$$\mathrm{d}s^2 = \mathrm{d}t^2 - e^{\frac{2t}{\alpha}} \left(\mathrm{d}x^2 + \mathrm{d}y^2 + \mathrm{d}z^2\right). \tag{2.16}$$

An investigation into the propagation of gravitational waves in vacuum with a positive cosmological constant (λ) was carried out in [9] and subsequently [10] by Bičák and Podolskỳ in 1999. In the former paper, they analysed the geometric properties of non-twisting type N solutions and in the later they discussed their physical properties. Their main focus in [10] was to analyse the equation of geodesic deviation and using the Newman-Penrose null tetrad and having analysed the said equation, they did show that the non-twisting N type solutions can be interpreted as transverse gravitational waves propagating in Minkowski, de Sitter or anti-de Sitter depending on the value assigned to λ . They further demonstrated that for a positive cosmological constant, an observer moving along the geodesics will witness waves decaying fast exponentially and the spacetime approaching de Sitter locally. On the contrary, in this work we seek to investigate the phenomena arising using waves which exhibit plane topology.

There are a number of earlier works on well-posedness of an initial boundary value problem for the Einstein's equations and among them is one by Friedrich and Nagy in 1999 [26]. In their article they prescribed initial data on an oriented 3-dimensional manifold and boundary conditions to this manifold. They went on to prescribe gauge source functions which described the evolution of the fields. Given that all data are smooth and consistency conditions are met on the boundaries, it was shown that there exists a smooth solution to the Einstein's vacuum equations $R_{ab} = \lambda g_{ab}$.

Substantial research in astronomy as in Hawking et al. [29] among others and observations made by renowned organisations like National Aeronautics and Space Administration (NASA), have provided enough evidence that the the universe is expanding at an accelerated rate. Efforts to measure this rate already exist in literature for instance in [19]. Recent researches by Woodard and Tsamis in 2014 [48] and earlier in 2013 [47] revealed that indeed gravitational radiation affects this expansion rate on an initial time slice. In particular, they found out that the introduction of gravitational radiation has the potential to slow down the expansion rate enough to stop the expansion or even make the universe contract. In this research we numerically investigate this finding, away from the initial hypersurface, using a similar expansion parameter derived in our ansatz as provided in Chapter 4.

Chapter 3

The Friedrich-Nagy gauge with cosmological constant and matter

The Friedrich-Nagy gauge, which was put forward by Friedrich and Nagy in [25, 26], is a formulation of the Einstein equations that employs the Newman-Penrose formalism discussed above. The spin-coefficients and curvature quantities are the variables in the Friedrich-Nagy representation of the Einstein equations. The gauge gives an initial boundary value problem (IBVP) formulation of the Einstein equations which is a symmetric-hyperbolic system and thus well-posed. The gauge therefore reduces the geometric initial boundary value problem for the Einstein field equations to a maximally dissipative initial boundary value problem. That is, boundary conditions are imposed (or not) based on the ingoing characteristic modes of the system, and do not add positively to the rate of change of the 'energy' of the system. Thus, we will write down the EFEs for our particular case in the Friedrich-Nagy gauge in the subsequent sections.

The aforementioned F-N gauge has rarely been implemented in numerical simulations as it is deemed to be too complicated. The only implementation to date was put forward by Frauendiener and Stevens in 2014 [24]. In their research they studied the numerical performance of the F-N gauge and the related boundary conditions considering a very simple case, that of colliding plane gravitational waves in Minkowski space-time. Frauendiener and Stevens concluded that their numerical implementation of the EFE as an IBVP in the F-N gauge is numerically stable. In this study we investigate the propagation of plane gravitational waves in the same way, but with the addition of a positive cosmological constant.

As stated earlier, the IBVP for the Einstein's equations is the basic tool used

in the numerical study of interaction of gravitational waves. In the upcoming section we present the derivation of the field equations in the Friedrich-Nagy gauge from the perspective of well-posedness of the IBVP. Here we closely follow the derivations put forward by Griffiths [28] and Frauendiener et al [24].

3.1 Gauge conditions

In order to permit the existence of gravitational waves in the spacetime, we assume that the spacetime (M, g) allows for the action of a two-dimensional translation group using isometries and also assume that the orbits foliate M and are $\mathbb{R}^2$ topologically.

On collision, the approaching waves which have plane symmetry will warp each other. In order to investigate this interaction of the gravitational plane waves we can introduce local coordinates (x, y) and initially assume the existence of Killing vectors represented as coordinate derivatives

$$\xi_1 = \partial_x, \quad \xi_2 = \partial_y \tag{3.1}$$

throughout the entire spacetime. Thus at each point of the manifold M, there are just two null directions which are orthogonal to the planes ($v = const$ and $u = const$) spanned by the Killing vectors ξ_1 and ξ_2. We can introduce a vector l^a that is orthogonal to the null hyper-plane $u = constant$ and likewise introduce vector n^a that is orthogonal to $v = constant$ with the assumption that these two vectors are normalised against each other i.e $l_a n^a = 1$. In addition to these real future-pointing null vectors, we choose a third complex null vector to span the hyperplanes and is defined as

$$m^a = \xi\partial_x + \eta\partial_y,$$

where ξ and η are functions that will be fixed later. For numerical computation, we need a suitable coordinate system which is attained by the introduction of local coordinates $t(u, v)$ and $z(u, v)$ which are constant on the planes. These are fixed by imposing the FN gauge conditions. First, we chose an initial spacelike hypersurface on which to prescribe initial data for the IBVP assuming that the Killing vectors are tangent to it. We then choose a timelike vector field t^a such

that it is tangent everywhere to the timelike boundaries (T_{-1} and T_1) set at $z = -1$ and $z = 1$ and so t^a is orthogonal to the constant z surfaces. To eliminate the remaining boost freedom we require that the unit vector t^a be proportional to the sum of the null vectors l^a and n^a that is

$$t^a = \alpha(l^a + n^a). \tag{3.2}$$

The value of α can be determined from the requirement of unit vectors as

$$\begin{aligned} & t^a t_a = 1 \\ & 1 = (\alpha(l^a + n^a))(\alpha(l_a + n_a)) \\ & 1 = \alpha^2(l^a l_a + l^a n_a + n^a l_a + n^a n_a) \\ & 1 = \alpha^2(1 + 0 + 0 + 1) \\ & 1 = 2\alpha^2 \\ & \Rightarrow \alpha = \tfrac{1}{\sqrt{2}} \end{aligned} \tag{3.3}$$

and so equation (3.3) becomes $t^a = \frac{1}{\sqrt{2}}(l^a + n^a)$. At this stage it can be noted that the unit vector t^a is yet to be fixed and so we can choose z in an arbitrary way. The natural way of achieving this is to choose them is such a way that they be orthogonal to the initial hypersurface. This freedom will be fixed by specifying the mean extrinsic curvature later in this study.

We then choose another spacelike unit vector z^a which is orthogonal to t^a and satisfying the inner product $t^a z_a = 0$. Likewise, z^a must be a linear combination of l^a and n^a as

$$z^a = Cl^a + Dn^a. \tag{3.4}$$

Again the values of C and D can be determined using the inner product requirement of unit vectors as follows

$$\begin{aligned} z^a z_a &= 1 \\ 1 &= (Cl^a + Dn^a)(Cl_a + Dn_a) \\ 1 &= 2CD \end{aligned}$$

$$\begin{aligned} \text{and taking into account the condition } t^a z_a &= 0 \\ \text{it follows that } C = -D &= \frac{1}{\sqrt{2}} \end{aligned}$$

and so (3.4) becomes

$$z^a = \frac{1}{\sqrt{2}}(l^a - n^a). \tag{3.5}$$

Having chosen the spatial coordinate z on our initial hypersurface, we now denote the other two remaining coordinates x and y. We then choose two spacelike unit vectors x^a and y^a in such a way that they are orthogonal to t^a and z^a. Since we have chosen m^a to span the planes we then have

$$m^a = \frac{1}{\sqrt{2}}(x^a + iy^a). \tag{3.6}$$

We need to check whether this satisfies inner product requirement for unit vectors

$$\begin{aligned} m^a m_a = 0 &= (\frac{1}{\sqrt{2}}(x^a + iy^a))(\frac{1}{\sqrt{2}}(x_a + iy_a)) \\ &= (x^a x_a - y^a y_a) + 2ix^a y_a \\ &= 2ix^a y_a \\ \Rightarrow x^a y_a &= 0. \end{aligned}$$

Thus x^a and y^a are orthogonal. Also to note is that

$$\begin{aligned} m^a \bar{m}_a &= \frac{1}{2}(x^a + iy^a)(x_a - iy_a) \\ &= \frac{1}{2}(x^a x_a + y^a y_a) = -1 \end{aligned}$$

This is as required from the null tetrad vector properties.

Extending the coordinate system everywhere in the neighbourhood of the timelike boundaries, we then choose t to be the parameter of the integral curves of t^a, that is

$$t^a \nabla_a t = 1 \Rightarrow t^a \nabla_a = t^a \partial_a = \partial_t.$$

Moreso, our conditions imply

$$z_a = -\frac{1}{A}\nabla_a z \Rightarrow z^a \nabla_a = B\partial_t + A\partial_z + X\partial_x + Y\partial_y$$

where $A(t,z), B(t,z), X(t,z)$ and $Y(t,z)$ are invariant functions. It had been shown in [24] that using the freedom in the choice of x and y, we can eliminate the functions X and Y and so we will ignore equations involving these. Having

defined a gauge with coordinates (t, x, y, z) and frame (t^a, x^a, y^a, z^a) we can now derive l^a and n^a using (3.2) and (3.5) as

$$t^a + z^a = \frac{2}{\sqrt{2}} l^a \qquad t^a - z^a = \tfrac{2}{\sqrt{2}} n^a$$
$$\Rightarrow l^a = \frac{1}{\sqrt{2}}(t^a + z^a) \qquad \Rightarrow n^a = \tfrac{1}{\sqrt{2}}(t^a - z^a).$$

From these we can represent the null tetrad (l^a, n^a, m^a) in terms of directional derivatives

$$D = l^a \nabla_a = \frac{1}{\sqrt{2}}((1+B)\partial_t + A\partial_z), \tag{3.7}$$
$$D' = n^a \nabla_a = \frac{1}{\sqrt{2}}((1-B)\partial_t - A\partial_z), \tag{3.8}$$
$$\delta = m^a \nabla_a = \xi \partial_x + \eta \partial_y \tag{3.9}$$

Here the complex spacelike vector m^a is given in terms of complex-valued functions $\xi(t, z)$ and $\eta(t, z)$. It is in these coordinates that the metric assumes the form

$$g = \left(\mathrm{d}t - \frac{B}{A}\mathrm{d}z\right)^2 - \frac{1}{A^2}\mathrm{d}z^2 + \frac{2}{(\xi\bar{\eta} - \bar{\xi}\eta)^2}(\eta \mathrm{d}x - \xi \mathrm{d}y)(\bar{\eta}\mathrm{d}x - \bar{\xi}\mathrm{d}y). \tag{3.10}$$

3.2 The field equations

The derivation of the field equations in the Newman-Penrose formalism involves the use of the commutator relations (2.5) put forward by Penrose and Rindler [39]. Acting these on to the coordinates (t, x, y, z) we obtain the relationships between the tetrad functions and the spin coefficients

$$\rho = \bar{\rho}, \quad \rho' = \bar{\rho}', \quad \kappa' = 0, \quad \kappa = 0, \quad \alpha = 0, \quad \beta = 0, \quad \tau = 0, \quad \tau' = 0,$$
$$(D + D')B = (\gamma + \bar{\gamma} + \epsilon + \bar{\epsilon}) + (\gamma + \bar{\gamma} - \epsilon - \bar{\epsilon})B,$$
$$(D + D')A = (\gamma + \bar{\gamma} - \epsilon - \bar{\epsilon})A,$$
$$(D + D')X = (\gamma + \bar{\gamma} - \epsilon - \bar{\epsilon})X,$$
$$(D + D')Y = (\gamma + \bar{\gamma} - \epsilon - \bar{\epsilon})Y,$$
$$D\xi = \sigma\bar{\xi} + (\epsilon - \bar{\epsilon} + \rho)\xi, \qquad D'\xi = \bar{\sigma}'\bar{\xi} + (\gamma - \bar{\gamma} + \rho')\xi,$$
$$D\eta = \sigma\bar{\eta} + (\epsilon - \bar{\epsilon} + \rho)\eta, \qquad D'\eta = \bar{\sigma}'\bar{\eta} + (\gamma - \bar{\gamma} + \rho')\eta. \tag{3.11}$$

We then come up with next set of equations put forward in [39] equation (4.11.12) which are curvature equations. These are derivatives in the direction of null vectors of spin coefficients given above and are known to contain information about curvature. Subject to the given simplifications together with non-zero cosmological constant as well as Ricci tensor components (i.e $\lambda \neq 0$, $\Phi_{ij} \neq 0$) they read

$$\begin{aligned}
D\rho &= \rho^2 + \sigma\bar{\sigma} + \rho(\epsilon + \bar{\epsilon}) + \Phi_{00}, \\
D'\rho' &= (\rho')^2 + \sigma'\bar{\sigma}' - \rho'(\gamma + \bar{\gamma}) + \Phi_{22}, \\
D\sigma &= 2\rho\sigma + \sigma(3\epsilon - \bar{\epsilon}) + \Psi_0, \\
D'\sigma' &= 2\rho'\sigma' - \sigma'(3\gamma - \bar{\gamma}) + \Psi_4, \\
D'\sigma &= \rho'\sigma + \bar{\sigma}'\rho + \sigma(3\gamma - \bar{\gamma}) - \Phi_{02}, \\
D\sigma' &= \rho\sigma' + \bar{\sigma}\rho' - \sigma'(3\epsilon - \bar{\epsilon}) - \Phi_{20}, \\
D'\rho &= \rho\bar{\rho}' + \sigma\sigma' + \rho(\gamma + \bar{\gamma}) - \Psi_2 - 2\Lambda, \\
D\rho' &= \rho'\bar{\rho} + \sigma\sigma' - \rho'(\epsilon + \bar{\epsilon}) - \Psi_2 - 2\Lambda, \\
D\gamma - D'\epsilon &= -\gamma(\epsilon + \bar{\epsilon}) - \epsilon(\gamma + \bar{\gamma}) + \Psi_2 + \Phi_{11} - \Lambda,
\end{aligned} \tag{3.12}$$

together with the algebraic conditions for the Weyl tensor components Ψ_1, Ψ_2 and Ψ_3 :

$$\Psi_1 = 0, \qquad \Psi_2 = \sigma\sigma' - \rho\rho' + \Phi_{11} + \Lambda, \qquad \Psi_3 = 0, \tag{3.13}$$

where Λ is the curvature scalar related to the cosmological constant by $6\Lambda = \lambda$ in vacuum.

From the Bianchi identity, $\nabla_{[a}R^{e}_{bc]d} = 0$, we obtain the final set of equations regarded as equations for the Weyl tensor components

$$\begin{aligned}
D\Psi_2 + D'\Phi_{00} - 2(\gamma + \bar{\gamma})\Phi_{00} + 2D\Lambda &= \sigma'\Psi_0 + 3\rho\Psi_2 + \bar{\rho}'\Phi_{00} + 2\rho\Phi_{11} + \bar{\sigma}\Phi_{02}, \\
D'\Psi_2 + D\Phi_{22} + 2(\epsilon + \bar{\epsilon})\Phi_{22} + 2D'\Lambda &= \sigma\Psi_4 + 3\rho'\Psi_2 + \bar{\rho}\Phi_{22} + 2\rho'\Phi_{11} + \bar{\sigma}'\Phi_{20}, \\
D\Psi_4 - 4\gamma'\Psi_4 + D'\Phi_{20} + 2(\gamma - \bar{\gamma})\Phi_{20} &= 3\sigma'\Psi_2 + \rho\Psi_4 + 2\sigma'\Phi_{11} + \bar{\rho}'\Phi_{20} + \bar{\sigma}\Phi_{22}, \\
D'\Psi_0 - 4\gamma\Psi_0 + D\Phi_{02} - 2(\epsilon - \bar{\epsilon})\Phi_{02} &= 3\sigma\Psi_2 + \rho'\Psi_0 + 2\sigma\Phi_{11} + \bar{\rho}\Phi_{02} + \bar{\sigma}'\Phi_{00}, \\
D\Phi_{11} + D'\Phi_{00} - 2(\gamma + \bar{\gamma})\Phi_{00} + 3D\Lambda &= 2\rho'\Phi_{00} + 2\rho\Phi_{11} + \sigma\Phi_{20} + \bar{\sigma}\Phi_{02}, \\
D'\Phi_{11} + D\Phi_{22} + 2(\epsilon + \bar{\epsilon})\Phi_{22} + 3D'\Lambda &= 2\rho\Phi_{22} + 2\rho'\Phi_{11} + \sigma'\Phi_{02} + \bar{\sigma}'\Phi_{20}.
\end{aligned} \tag{3.14}$$

We face a problem, we have twenty variables and fifteen equations. We turn

back to the F-N gauge conditions imposed earlier and first determine the mean curvature of the timelike boundaries in terms of spin coefficients as

$$\begin{aligned}\chi &= (g^{ab} + z^a z^b)\nabla_a z_b \\ &= \frac{1}{\sqrt{2}}(\epsilon + \bar{\epsilon} + \gamma + \bar{\gamma} - 2\rho + 2\rho').\end{aligned} \tag{3.15}$$

From the symmetry assumptions, it can be noted that the Fermi transport **F** of the space-like unit vectors x^a and y^a (and consequently of m^a) along the time-like unit vector t^a reduces to parallel transport and so

$$\begin{aligned}\mathbf{F}m^a &= t^c\nabla_c m^a \\ &= \frac{1}{\sqrt{2}}(\epsilon - \bar{\epsilon} + \gamma - \bar{\gamma})m^a.\end{aligned} \tag{3.16}$$

The remaining gauge freedom in choosing m^a is determined by using

$$\mathbf{F}m^a = \beta f m^a$$

where f is an arbitrary real valued invariant function of t and z. Combining (3.15) and (3.16) we get

$$\epsilon + \gamma = \rho - \rho' + F, \tag{3.17}$$

with $F(t, z)$ being an invariant complex valued function where $\sqrt{2}F = \chi + \beta f$. If we introduce another complex valued function $\mu(t, z)$ defined as

$$\mu = \gamma - \epsilon, \tag{3.18}$$

then we can explicitly express ϵ and γ in terms of μ and F which yields the following $\epsilon - \gamma$ rules in terms of freely specifiable complex-valued functions $F(t, z)$ and $\mu(t, z)$ as;

$$\epsilon = \frac{1}{2}(\rho - \rho' + F - \mu), \qquad \gamma = \frac{1}{2}(\rho - \rho' + F + \mu). \tag{3.19}$$

If then we insert these expressions into the last of the curvature equations (3.12) above, we obtain an equation for the function μ as;

$$\begin{aligned}(D + D')\mu = {} & D'F - DF + \mu(\mu + \rho) + \bar{\mu}(\mu + \rho + \rho') + \rho'(3F + \mu + 8\rho + \bar{F}) \\ & - F^2 - 2\Lambda - 3\rho(F + \rho) - \bar{F}(F + \rho) - \sigma\bar{\sigma} - 3(\rho')^2 - \bar{\sigma}'\sigma \\ & + 2\Phi_{11} + 2\Psi_2.\end{aligned} \tag{3.20}$$

3.2.1 Evolution equations

The final step is to split the equations obtained above into evolution and constraint equations. First, we substitute ϵ and γ given in (3.19) as well as replacing D and D' into the first two equations in (3.11) above to get evolution equations for the metric functions A and B as the first two equations in (3.21) below. We ignore the rest of the equations involving functions ξ and η because equations for these decouple from the system and could be determined once the other remaining equations have been solved. Doing the same for the curvature equations in (3.12) and combining them appropriately we obtain the rest of the evolution equations below (3.21) for the divergences ρ and ρ', shears σ and σ', μ, the Ricci tensor components Φ_{ij} as well as the Weyl tensor components Ψ_0 and Ψ_4 as

$$
\begin{aligned}
\sqrt{2}\partial_t A &= A(\mu+\bar{\mu}),\\
\sqrt{2}\partial_t B &= (F+\bar{F}+2\rho-2\rho') + (\bar{\mu}+\mu)B,\\
\sqrt{2}\partial_t \rho &= 3\rho^2+\sigma\bar{\sigma}+\rho(F+\bar{F})-3\Lambda+\Phi_{00}-\Phi_{11},\\
\sqrt{2}\partial_t \rho' &= 3(\rho')^2+\sigma'\bar{\sigma}'-\rho'(F+\bar{F})-3\Lambda+\Phi_{22}-\Phi_{11},\\
\sqrt{2}\partial_t \sigma &= 4\rho\sigma-\sigma\rho'+\rho\bar{\sigma}'+\sigma(3F-F)+\Psi_0,\\
\sqrt{2}\partial_t \sigma' &= 4\rho'\sigma'-\sigma'\rho+\rho'\bar{\sigma}-\sigma'(3F-F)+\Psi_4,\\
\sqrt{2}\partial_t \mu &= \mu^2+\mu\bar{\mu}-3(\rho-\rho')^2+(\mu+\bar{\mu})(\rho+\rho')-\sigma\bar{\sigma}-\sigma'\bar{\sigma}'+2\sigma\sigma'\\
&\quad -(\rho-\rho')(\bar{F}+3F)-F^2-FF-\sqrt{2}A\partial_z F\\
&\quad -\sqrt{2}B\partial_t F-6\Lambda-\Phi_{00}+2\Phi_{11}-\Phi_{22},\\
(1-B)\partial_t\Psi_0-A\partial_z\Psi_0 &= \sqrt{2}\Big[\sigma(3\Lambda+5\Phi_{11}-3\rho\rho'+3\sigma\sigma')\\
&\qquad +(2F+2\mu+2\rho-\rho')\Psi_0+\Phi_{00}\bar{\sigma}'\Big],\\
(1+B)\partial_t\Psi_4+A\partial_z\Psi_4 &= \sqrt{2}\Big[\sigma'(3\Lambda+5\Phi_{11}-3\rho\rho'+3\sigma\sigma')\\
&\qquad +(-2F+2\mu+2\rho'-\rho)\Psi_4+\Phi_{22}\bar{\sigma}\Big].
\end{aligned}
\tag{3.21}
$$

3.2.2 The constraint equations and the subsidiary system

The remaining equations after identifying the evolution equations can be written as the vanishing of constraint quantities C_i. These are those equations not containing time derivatives thus are defined on each slice of constant time as

$$\begin{aligned}
C_1 &= -\frac{1}{\sqrt{2}A}\Big[3(1+B)\Lambda - \rho(\mu - \rho + B(F+3\rho)) - B\rho\bar{F} \\
&\quad - (-1+B)\sigma\bar{\sigma} - \rho(\bar{\mu} + 2\rho^*)\Big] + \partial_z(\rho), \\
C_2 &= -\frac{1}{\sqrt{2}A}\Big[-3BF + 3\mu - 2\rho + 4B\rho)\sigma + B\sigma\bar{F} - (1+B)\rho\overline{\sigma^*} \\
&\quad - (-1+B)\Psi_0 + \sigma(\bar{\mu} + (-1+B)\rho^*)\Big] + \partial_z(\sigma), \\
C_3 &= -\frac{1}{\sqrt{2}A}\Big[3(1+\bar{B})\bar{\Lambda} - F\bar{B}\bar{\rho} - \bar{\rho}(\bar{\mu} - \bar{\rho} + \bar{B}(\bar{F}+3\bar{\rho})) \\
&\quad - \sigma(-1+\bar{B})\bar{\sigma} - \bar{\rho}(\mu + 2\overline{\rho^*})\Big] + \partial_z(\bar{\rho}), \\
C_4 &= -\frac{1}{\sqrt{2}A}\Big[F\bar{B}\bar{\sigma} - (3\bar{B}\bar{F} + 3\bar{\mu} - 2\bar{\rho} + 4\bar{B}\bar{\rho})\bar{\sigma} - (-1+\bar{B})\overline{\Psi_0} \\
&\quad + \bar{\sigma}(\mu + (-1+\bar{B})\overline{\rho^*}) - (1+\bar{B})\bar{\rho}
\end{aligned} \tag{3.22}$$

We then check for constraint propagation, i.e. how the constraints propagate from one time slice to the other. We do so by taking the time derivatives,$\partial_t[C_i]$, of the constraint equations above taking into account the fact that $\partial_t\Lambda = 0$, $\partial_z\Lambda = 0$ together with other necessary simplifications we have

$$\begin{aligned}
\sqrt{2}T(C_1) &= \sigma\overline{C_3} + C_1(F + 6\rho + \bar{F}) + \bar{\sigma}C_3, \\
\sqrt{2}T(C_2) &= \overline{\sigma^*}C_4 + C_2(-F - \bar{F} + 6\rho^*) + \overline{C_4}\sigma^*, \\
\sqrt{2}T(C_3) &= \rho\overline{C_4} + C_1(4\sigma + \overline{\sigma^*}) - \sigma C_2 + C_3(3F + 4\rho - \overline{F} - \rho^*), \\
\sqrt{2}T(C_4) &= \overline{C_3}\rho^* + C_4(-3F - \rho + \overline{F} + 4\rho^*) - C_1\sigma^* + C_2(\overline{\sigma} + 4\sigma^*).
\end{aligned} \tag{3.23}$$

and the result above are equations involving combinations of the constraints themselves. Thus if C_i are zero initially, they will remain zero. The constraint quantities do propagate within the hypersurfaces only and they do not cross the constant z boundaries. This then means that the only boundary conditions to be imposed are those for the Weyl tensor components Ψ_4 and Ψ_0.

3.3 The expansion parameter H.

Here we derive the expansion parameter in our ansatz. The standard definition of the expansion rate H as in [29],[47],[48] in terms of a covariant derivative, ∇^a, of a timelike 4-velocity co-vector field $(\mathrm{d}t)_a$:

$$\begin{aligned} H &= \frac{1}{3}\nabla^a(\mathrm{d}t)_a \\ &= \frac{1}{3}g^{ab}\nabla_b(\mathrm{d}t)_a \end{aligned} \tag{3.24}$$

From equations (3.7) in the proceeding section, we have expressions for the null vectors l^a and n^a as

$$l^a = \frac{1}{\sqrt{2}}((1+B)\partial_t + A\partial_z) \tag{3.25}$$

$$n^a = \frac{1}{\sqrt{2}}((1-B)\partial_t - A\partial_z) \tag{3.26}$$

Since these are normalised against each other such that $l^a l_a = 0$ and $l_a n^a = 1$, we obtain

$$l_a = \frac{1}{\sqrt{2}}\mathrm{d}t - \frac{1}{\sqrt{2}}\frac{(1+B)}{A}\mathrm{d}z \tag{3.27}$$

$$n_a = \frac{1}{\sqrt{2}}\mathrm{d}t + \frac{1}{\sqrt{2}}\frac{(1-B)}{A}\mathrm{d}z \tag{3.28}$$

Adding (3.27) and (3.28) above we have

$$l_a + n_a = \sqrt{2}\mathrm{d}t - \sqrt{2}\frac{B}{A}\mathrm{d}z \tag{3.29}$$

Subtracting (3.27) and (3.28) and solving for $\mathrm{d}z$, substituting the result into (3.29) above yields

$$\mathrm{d}t = \frac{1}{\sqrt{2}}((1-B)l_a + (1+B)n_a) \tag{3.30}$$

substituting (3.30) into definition (3.24) and simplyfying yields

$$H = \frac{1}{3}(l^a n^b + n^a l^b - m^a\overline{m}^b - \bar{m}^a m^b)\nabla_b[\frac{1}{\sqrt{2}}((1-B)l_a + (1+B)n_a)]_a \tag{3.31}$$

expanding the above and simplifying it subject to the definitions put forward in [39], Eq. (4.5.21) through to Eq. (4.5.23) we have

$$H = \frac{1}{3}\left[\frac{1}{\sqrt{2}}\Big[(1+B)(\epsilon' + \bar{\epsilon}' - 2\rho') + (1-B)(\epsilon + \bar{\epsilon} - 2\rho) + D'B - DB\Big]\right] \tag{3.32}$$

Now taking into account the $\epsilon - \gamma$ rules derived earlier in Eq. (3.19) together with definitions (3.7) and (3.8) the above expression simplifies to

$$H = \frac{1}{3}\left[-\sqrt{2}\Big(\rho + \rho' + \frac{1}{2}(\mu + \bar{\mu})\Big) - \frac{B}{\sqrt{2}}(F + \bar{F}) - (B\dot{B} + AB')\right]. \tag{3.33}$$

This is the expansion rate to be numerically implemented in our code and the results will be discussed in the following chapter.

3.4 The Kretschmann Scalar I

In general relativity applications, the Kretschmann scalar I is a quadratic polynomial scalar invariant first introduced by Erich Kretschmann. It is said to be quadratic as it can be expressed as a sum of squares of tensor components. It is sometimes referred to as the square of the Riemann curvature tensor, in other words

$$I = R_{abcd}R^{abcd} \tag{3.34}$$

where R_{abcd} is the Riemann tensor. An equivalent expression for this curvature invariant in the Newman-Penrose formalism to be implement in our code is

$$I = 2\Psi_0\Psi_4 + 6(\Psi_2)^2, \tag{3.35}$$

using that $\Psi_1 = 0 = \Psi_3$. It shall be computed during the evolutions together with the other system variables and later analysed in Chapter 5.

Part II

Numerical Implementation

Chapter 4

The numerical setup

4.1 The Python package COFFEE

Recently, the relativity group at the University of Otago developed a Python package called COFFEE, an acronym for COnFormal Field Equation Evolver, although being able to evolve generic partial differential equations [20]. This was developed to numerically evolve systems of hyperbolic partial differential equations over time using the method of lines. It comprises of time integrators and finite differencing stencils with the summation-by-parts property. In addition the package has a pseudo-spectral functionality for angular derivatives of spin-weighted functions. Generally COFFEE does not require much from users and was written with PEP8 [20] as the guiding philosophy. Additional advantages of this numerical integrator are that it is Message Passing Interface (MPI)-parallelisable on a variety of different geometries, offers Hierarchical Data Format (HDF) data output and post processing scripts to visualise data. This functionality has given rise to its recent uses in the numerical studies of conformal properties of general relativity put forward in [7], [21], [5], [6], [4], [24], [22], [8]. According to the findings of Frauendiener and Stevens in their research project [24], COFFEE can reliably be used in the numerical study of propagating and colliding plane gravitational waves. In addition the package has pseudo-spectral functionality for angular derivatives of spin-weighted functions, however we do not use them here. In this study we are dealing with complex and challenging systems of equations derived from the Einstein's field equations and so we shall use COFFEE, a software built on the principle of user-friendliness and flexibility.

4.2 Numerical description

We arrived at a IBVP formulation of the Einstein equations realised by the Friedrich-Nagy gauge in the preceding sections. This is a finite system and so we need to discretise our computational domain in the z-direction. We discretise our z-grid into equidistant points in the interval [-1,1]. Furthermore we discretise the time direction into equidistant points in which the stepsize h_t is related to the stepsize for the z-direction h_z by $h_t = Ch_z$, where C denotes the Courant number. This number is meant to satisfy the Courant-Friedrichs-Levy (CFL) condition [16] in order to attain stable evolutions. Unless otherwise stated we take the CFL condition to be 0.5 which means that together with the special discretisation that fixes the temporal stepsize this fixes our grid. Then on this organised grid we will put our equations.

The main idea is to prescribe some initial data for the system variables on a chosen hyper-surface in such a way that the constrains C_i (3.22) are satisfied. We then evolve this initial data using evolution equations (3.21) and boundary conditions are carefully chosen to avoid constraint violation throughout the period of evolution. In order to achieve this, our system is discretised first using the method of lines. This is done in order to evolve the system on a computer using numerical methods.

The method of lines (MOL) has been commonly used in numerical codes developed for solving systems of differential equations. Conceptually, MOL discretises the space dimension while leaving time continous. This results in an ODE in time to be solved at each spatial grid point, which we solve using, for instance a Runge-Kutta method. The commonly used fourth-order Runge-Kutta method (RK4) has a broad stability range for a variety of hyperbolic problems. To demonstrate this as in [3], we consider an initial value problem of the form

$$\frac{du}{dt} = f(u,t), \quad u(t_0) = u_0 \tag{4.1}$$

for a function u. Then for a step-size $\Delta t > 0$, the value of the function u at the next time-step (u^{n+1}) using the RK4 method is

$$u^{n+1} = u^n + \frac{\Delta t}{6}(k_1 + 2k_2 + 2k_3 + k_4), \tag{4.2}$$

where

$$k_1 = f(u_n, t_n) \tag{4.3}$$

$$k_2 = f\Big(u_n + k_1\frac{\Delta t}{2}, t_n + \frac{\Delta t}{2}\Big) \tag{4.4}$$

$$k_3 = f\Big(u_n + k_2\frac{\Delta t}{2}, t_n + \frac{\Delta t}{2}\Big) \tag{4.5}$$

$$k_4 = f\Big(u_n + k_3\Delta t, t_n + \Delta t\Big). \tag{4.6}$$

Hence the method of lines obtained in this way, MOL-RK4, consists of four evaluations of the RHS of the PDEs at each grid point in order to move forward once in time. The method can be shown to be fourth order accurate in time.

The spatial finite differencing operators to be used in our case are the summation-by-parts (SBP) operators put forward by Kreiss in 1974 [32]. The SBP are analogous to integration by parts but discrete and are conventionally known to consists of centered difference interior schemes. The boundary stencils are designed to satisfy a discrete version of initial boundary problem (IBP) and these are usually imposed by the simultaneous-approximation term (SAT) method [46]. The combination SBP-SAT, known to be stable and accurate for long time simulations, has proven to be a powerful framework for treating the boundaries as proved by its wide use for instance in [7],[18] [33] and more recently in [24],[27].

4.2.1 SBP finite difference operators

Here we present the SBP finite difference operators used to approximate a first order derivative operator. We are dealing with PDEs emanating from EFEs which are hyperbolic equations however we shall use a simple advection to explore methods for hyperbolic problems. Consider a simple 1D advection equation

$$u_t = \alpha u_z, \quad \text{in} \quad [0, \infty) \times [z_0, z_N] \tag{4.7}$$

where z and s are real numbers, α is a non-zero constant, z_0 and z_N are the left and right boundaries respectively, u is a differential function in the space of real

integrable functions $L^2[z_0, z_N]$. In this discussion we wish to approximate the spatial derivative operator $\frac{\partial}{\partial z}$ using finite differencing. We now define

$$(u, v) := \int_{z_0}^{z_N} (uv) \mathrm{d}z,$$

thus the L^2-norm of u is given as

$$||u|| := \sqrt{\int_{z_0}^{z_N} (u^2) \mathrm{d}z}.$$

An estimate of the energy of the system is obtained by looking at the derivative of the L^2-norm of u with respect to time and using integration by parts together with (4.7) we get

$$\begin{aligned}
\frac{\mathrm{d}}{\mathrm{d}t}||u||^2 &= \frac{\mathrm{d}}{\mathrm{d}t} \int_{z_0}^{z_N} (u^2) \mathrm{d}z \\
&= \int_{z_0}^{z_N} \Big[(u_t u) + (u u_t) \Big] \mathrm{d}z \\
&= \int_{z_0}^{z_N} (u_t u) \mathrm{d}z + \int_{z_0}^{z_N} (u u_t) \mathrm{d}z \\
&= \alpha \int_{z_0}^{z_N} (u_z u) \mathrm{d}z + \alpha \int_{z_0}^{z_N} (u u_z) \mathrm{d}z \\
&= \alpha u^2 \Big|_{z_0}^{z_N} \\
&= \alpha \Big(u(t, z_N)^2 - u(t, z_0)^2 \Big)
\end{aligned} \tag{4.8}$$

where the last equality arises from IBP. The method is designed to ensure that the energy estimate is non-increasing so that it remains stable. To achieve this for $\alpha > 0$, we set the boundary condition $u(t, z_N) = 0$ and leave $u(t, z_0)$ free thus for the case $\alpha < 0$ we do exactly the opposite. Now, in order for us to get a similar estimate of the discretised equation's energy, we discretise the $z-$derivative operator. First we discretise u into $N+1$ equidistant points denoted by $v := \{v_0, v_1, ..., v_N\}$ and then denote the discretised norm by $||v||_H := v^T H v$, where H is a $(N+1) \times (N+1)$ positive-definite symmetric matrix. Then we can define the derivative operator as $D := H^{-1}Q$ where Q is a $(N+1) \times (N+1)$ matrix of constant entries. With this we can have the discretised equation as

$$v_t = \alpha D v \tag{4.9}$$

for which the energy estimate becomes

$$\frac{\mathrm{d}}{\mathrm{d}t}||v||_H^2 = \frac{\mathrm{d}}{\mathrm{d}t}\Big(v^T H v\Big) = \alpha v^T \Big(Q^T (H^{-1})^T H + Q \Big) v = \alpha v^T \Big(Q^T + Q \Big) v. \tag{4.10}$$

In order to obtain a similar form of the energy estimate (4.8) given earlier, we then restrict Q by the condition that

$$Q + Q^T = diag(-1, 0, ..., 0, 1) \tag{4.11}$$

which then implies that the energy estimate can be expressed as

$$\frac{\mathrm{d}}{\mathrm{d}t}||v||_H^2 = \alpha\Big(v_N^2 - v_0^2\Big). \tag{4.12}$$

Clearly it is the discretised equivalent of the energy estimate for the system (4.8)

As explained in [46], any finite difference operator $D := H^{-1}Q$ in which $H = H^T$, is said to exhibit the summation-by-parts property which guarantees numerical stability.

4.3 Boundary conditions

As mentioned earlier, the only boundary conditions to be imposed for our system are those for Ψ_0 (right boundary) and Ψ_4 (left boundary). It is shown in Friedrich-Nagy [26] that if we take non-reflecting boundary conditions, these functions can be prescribed arbitrarily. Numerically, we impose the boundary conditions using the simultaneous-approximation-term (SAT) method discussed by Carpenter, Nordström and Gottlieb in [13]. The SAT method requires the addition of a penalty term, which is weighted, to each of the evolution equations in such a way that the functions will be driven towards a desired value at the left (z_0) and right (z_N) boundaries.

In order to illustrate how the SAT method is implemented we adopt the one-dimensional problem (4.7) used previously and will then impose data on z_N, the right boundary. We wish to solve (4.7) taking into account the Dirichlet boundary condition

$$u(t, z_N) = g_N(t) \tag{4.13}$$

In order to drive the solution to the predetermined boundary value, we add a penalty term to the right hand side of the evolution equation (i.e (4.7)). We again introduce a parameter τ which determines the rate at which the solution

is driven to this prescribed value on the boundary. Using (4.13)) the boundary condition, the energy estimate for the system (4.8) becomes

$$\frac{\mathrm{d}}{\mathrm{d}t}||u||_H^2 = \alpha\Big(g_N(t)^2 - u(t,z_0)^2\Big) \tag{4.14}$$

As explained above, we then modify D to get the new equation for v as

$$v_t = \alpha H^{-1}Qv - \tau\alpha H^{-1}\Big(E_N v - e_N g_N(t)\Big), \tag{4.15}$$

where $E_N = diag(0,0,...,0,1)$ is an $(N+1)\times(N+1)$ matrix, τ is the penalty term and $e_N = (0,0,...,0,1)$. The method proves to be stable by choosing $\tau \geq 1$. Finally the energy estimate after imposing the SAT method is given by

$$\frac{\mathrm{d}}{\mathrm{d}t}||v||_H^2 = \alpha H^{-1}\Big(Q_v - \tau g_N(t)^2 E_N v_N\Big) + \mathbf{T}_e, \tag{4.16}$$

where $\mathbf{T}_e$ is the truncation error. In this work we choose $\tau = 1$.

4.4 Implementation of the SBP finite difference operators and the SAT method

The SBP finite difference operator implemented in COFFEE in our case is known as `D43_Strand` [46] derived from the fact that it is fourth order accurate in the interior and third order accurate on the boundaries. This inherits from a base class called `SBP` contained in COFFEE that contains methods relevant to any finite difference operator, such as the calculation routine. The calculation routine first checks to see if the grid is large enough to contain the chosen finite difference operator. It then computes the derivative on the entire interior part of the grid. It then updates the derivatives close to the boundaries where the finite difference stencil does not fit, by using a different stencil Q.

For the interior stencil, we use the standard centralised finite differencing stencil with weights $\{-1/12, 2/3, 0, -2/3, 1/12\}$ to approximate the first derivative of some function f at the point x_i. For example,

$$f'(x_i) \approx -\frac{1}{12}f(x_{i-2}) + \frac{2}{3}f(x_{i-1}) - \frac{2}{3}f(x_{i+1}) + \frac{1}{12}f(x_{i+2}). \tag{4.17}$$

The `D43_Strand` subclass contains the 5×7 matrix Q, which is used to evaluate the derivative at the boundary and the four points immediately interior, using

the function evaluated at the boundary and the six points immediately interior. The matrix Q is obtained according to the prescription of Strand (see [46] page 66.).

The implementation of the SAT method is more straightforward, whereby we simply modify the evolution equations, for the functions needed a boundary condition, at the boundary points. This is done by adding to the evolution equations there the difference of the numerical value of the function with the desired boundary condition, multiplied by τ, the characteristic speed and a value P. We choose $\tau = 1$, and the value of P comes again from Strand [46], which is $P = \frac{11}{3}\frac{1}{h_z}$, where h_z is the step size in the z-direction.

Part III

Results

Chapter 5

Results

In this chapter we fix (with the exception of the convergence tests) the spatial resolution to be 401 grid points. The CFL condition, put forward in [16] which is a requirement for a stable evolution, is set to 0.5. This then fixes the timestep to be $h_t = 0.5h_z = 0.5(2/400) = 0.0025$ where h_z is our spatial stepsize. We now need to prescribe initial data, boundary data and choose the gauge source function F. For the latter, we initially choose it to match the gauge of the exact spacetime used as initial data, which for all our cases is $F = 0$. We extend this to the entire space-time by requiring $F(t, z) = 0$ throughout. Also in this section we now refer to Λ as the cosmological constant for convenience, where in our case we have that $6\Lambda = \lambda$ as stated earlier.

5.1 Initial data

As emphasised by Cook in [15], initial data are the starting point for any numerical simulation, we therefore put forward the initial data for our system variables in Minkowski and de Sitter spacetimes. These initial data sets automatically satisfy the constraints (3.22) as they are solutions to the Einstein equations. We will shrink the z-direction for later convenience in both initial data sets by choosing $A = 4$. Note that $B = 0$ initially means that the t and z directions are orthogonal, but this will not always be the case once the space-times are gravitationally perturbed.

5.1.1 Initial data for Minkowski spacetime

Here we state the initial data at $t = 0$ for Minkowski space-time, which we take to be

$$g = (dt)^2 - \frac{1}{16}\Big((dx)^2 + (dy)^2 + (dz)^2\Big). \tag{5.1}$$

The initial data for our system obtained from this metric is given as

$$\begin{aligned} \Lambda &= 0, & B &= 0, \\ A &= 4, & \mu &= 0, \\ \sigma &= 0, & \rho &= 0, \\ \sigma' &= 0, & \rho' &= 0, \\ \Psi_0 &= 0, & \xi &= 2\sqrt{2}, \\ \Psi_4 &= 0, & \eta &= 2\sqrt{2}i. \end{aligned} \tag{5.2}$$

5.1.2 Initial data for de Sitter spacetime

In order to be compatible with our metric ansatz (3.10), we take de Sitter written in spatially Euclidean coordinates, which takes the form (2.16), namely

$$\mathrm{d}s^2 = \mathrm{d}t^2 - e^{\frac{2t}{\alpha}}\left(\mathrm{d}x^2 + \mathrm{d}y^2 + \mathrm{d}z^2\right). \tag{5.3}$$

This form of the metric yields the following initial data for $t = 0$

$$\begin{aligned} \Lambda &= 0.5, & B &= 0, \\ A &= 4, & \mu &= \pm\sqrt{\Lambda}, \\ \sigma &= 0, & \rho &= \pm\sqrt{\Lambda}, \\ \sigma' &= 0, & \rho' &= \pm\sqrt{\Lambda}, \\ \Psi_0 &= 0, & \xi &= 2\sqrt{2}, \\ \Psi_4 &= 0, & \eta &= 2\sqrt{2}i. \end{aligned} \tag{5.4}$$

Note the two possible sets of initial data for ρ, ρ' and μ. The explanation for this comes from the fact that α appearing in the line element is given by

$$\alpha^2 = \frac{1}{2\Lambda},$$

thus making the exponential term $e^{\pm 2\sqrt{2\Lambda}}$. This implies that the freedom in the choice of α in terms of Λ boils down to whether our universe is contracting or expanding. This can be compared to the signs of ρ and ρ', which when $\alpha = \frac{1}{\sqrt{2\Lambda}}$, are positive. Hence null congruences along both l^a and n^a are initially converging as expected from a comparison with the exponential term.

As we are interested in an expanding universe, we take ρ, ρ' and μ to be $-\sqrt{\Lambda}$.

5.2 Computation of null coordinates

Here we derive expressions for a choice of null coordinates (u, v) for the de Sitter and Minkowski spacetimes. Considering de Sitter for now, the null coordinates must satisfy

$$Du = 0, \qquad D'v = 0. \tag{5.5}$$

Replacing the directional derivatives in the l^a and n^a directions with t and z coordinate derivatives using Eqs. (3.7) and (3.8) we obtain

$$\frac{\partial u}{\partial t} + \frac{A}{1+B}\frac{\partial u}{\partial z} = 0 \quad \text{and} \quad \frac{\partial v}{\partial t} - \frac{A}{1-B}\frac{\partial v}{\partial z} = 0. \tag{5.6}$$

Now the de Sitter spacetime can be partly covered by

$$\mathrm{d}s^2 = \mathrm{d}t^2 - A_0^{-2} e^{2Ht}\left(\mathrm{d}x^2 + \mathrm{d}y^2 + \mathrm{d}z^2\right), H^2 = \lambda/3 \tag{5.7}$$

where A_0 is a scale for the spatial directions and H being the expansion parameter. Comparing this metric to our ansatz Eqn (3.10) we can determine the conditions for the metric functions A and B as

$$A = A_0 e^{-Ht}, \quad B = 0, \tag{5.8}$$

which when substituted into Eqn (5.6) gives

$$\frac{\partial u}{\partial t} + A_0 e^{-Ht}\frac{\partial u}{\partial z} = 0 \quad \text{and} \quad \frac{\partial v}{\partial t} - A_0 e^{-Ht}\frac{\partial v}{\partial z} = 0. \tag{5.9}$$

Solving such transport equations yield the general solutions which we fix by

$$u = \frac{1}{\sqrt{2}}\left[\frac{(1-e^{-Ht})}{H} - \frac{1+z}{A_0}\right] \tag{5.10}$$

$$v = \frac{1}{\sqrt{2}}\left[\frac{(1-e^{-Ht})}{H} - \frac{1-z}{A_0}\right]. \tag{5.11}$$

The above result has the consequence that initially at the boundaries u(0,-1) = v(0,1) = 0.

Going through the above procedure with the Minkowski metric will yield the same results as if we set our exponential term to one. Thus the null coordinates in Minkowski space-time are given by

$$u = -\frac{1}{\sqrt{2}}\left(\frac{1+z}{A_0}\right) + \frac{t}{\sqrt{2}} \tag{5.12}$$

$$v = -\frac{1}{\sqrt{2}}\left(\frac{1-z}{A_0}\right) + \frac{t}{\sqrt{2}}. \tag{5.13}$$

Further, we can define new quasi-invariant t and z coordinates T, Z by

$$T := \frac{v+u}{\sqrt{2}}, \qquad Z := \frac{v-u}{\sqrt{2}}, \tag{5.14}$$

which will allow us to produce plots of the Penrose-Carter variety later, where null rays are given by lines with 45 degree slopes.

5.3 Boundary data

Our system involves only four PDEs, namely the equations for the ingoing and outgoing gravitational plane waves ψ_0 and ψ_4 respectively and the two null coordinates. As we are interested in what phenomena arise when there is a single wave propagating, we only consider the propagation of Ψ_0 from the right boundary, i.e. $\psi_4(t,-1) = 0$. Thus we are left with the following boundary data to fix:

$$u(t,-1) = u_l(t), \qquad v(t,1) = v_r(t), \qquad \Psi_0(t,1) = \Psi_l(t). \tag{5.15}$$

First we fix the null coordinate's boundary data by injecting the exact solution's data there. I.e. we use

$$u_l(t) = v_r(t) = \frac{t}{\sqrt{2}}, \tag{5.16}$$

for Minkowski space-time and

$$u_l(t) = v_r(t) = \frac{\alpha(1 - e^{-\frac{t}{\alpha}})}{\sqrt{2}}. \tag{5.17}$$

for de Sitter. We take the wave profile for ψ_0 to be

$$\Psi_l(t) = \begin{cases} 32a\sin^8(bt),\ 0 < t < \dfrac{\pi}{b} \\ 0 \text{ otherwise} \end{cases} \tag{5.18}$$

where a and b are the wave amplitude and phase angle respectively. We choose $b = 35\pi/4$ so the area of the incoming wave is given by

$$\text{Area of } \Psi_0(t) = \int_0^{\frac{\pi}{b}} 32a\sin^8(bt)\,\mathrm{d}t = a \tag{5.19}$$

This is one way of putting forward the notion of energy of a gravitational wave in General Relativity. Schutz in [44] highlights that the question of energy in gravitational waves is a delicate one as it is not possible to localize the energy of the radiation to within a wavelength but rather an amount of stress-energy of a gravitational wave can be contained in an area of space which extends over several wavelengths.

5.4 Checks for correctness

Before experimenting with our code, which implements the system described in Chapter 4, checks for correctness must be carried out to validate it. To achieve this, we use de Sitter initial data and boundary data from the previous two

sections, where we use the same wave profile for the Ψ_4 boundary data to fully stress the system. This setup then describes colliding plane gravitational waves in de Sitter, where all system variables become non-trivial. Runs were carried out with resolutions of $100, 200, 400, 800$ and 1600 intervals in the z-direction. See fig (5.1) below for screenshots of the simulation with 400 intervals.

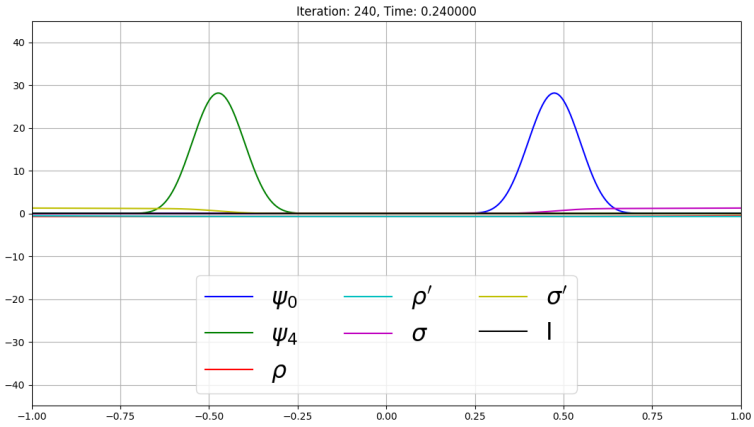

Figure 5.1: A screenshot of an ingoing and outgoing wave in de Sitter before their collision.

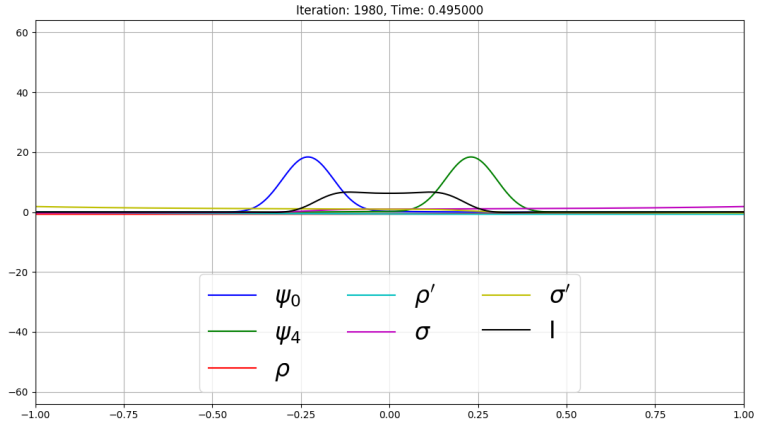

Figure 5.2: A screenshot of an ingoing and outgoing wave in de Sitter after their collision.

From the figure above, Ψ_4 and Ψ_0 indicate the wave fronts approaching each other from the left and right boundaries respectively. The parameters ρ,ρ',σ,σ' and I are plotted, which are the most physically meaningful system variables and scalar curvature invariant.

We now do multiple convergence tests to check that our constraints behave well and our system converges at the correct order. We focus on the constraint C_0 for this analysis, with results being nearly identical to the other constraints.

First we check how the constraints behave over time. In Fig. (5.3) we show the $\log_{10}$ of the L^2-norm of constraint $|C_0|$ as given in Eq. (3.22) over the course of the simulation.

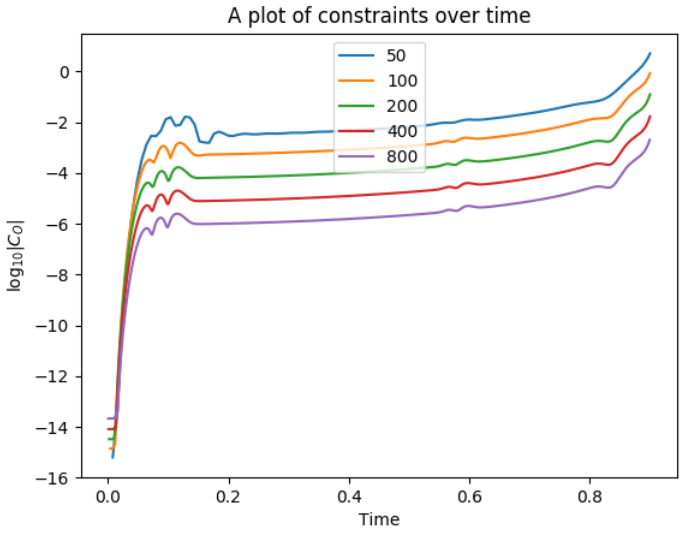

Figure 5.3: Constraint violation for C_o over time

It is clear that the L^2-norm of the constraint converges with increasing resolution, and that it is well behaved over time.

Now to see how the constraints converge on a t =constant slice. Toward this, we plot the $\log_{10}$ of $|C_0|$ in Fig. (5.4)

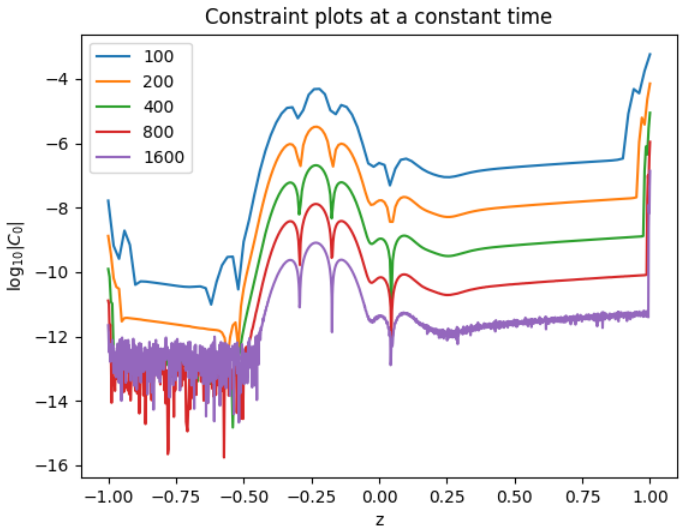

Figure 5.4: $\log_{10}|C_0|$ for all resolutions at $t = 0.4$.

It is clear that the constraints converge over the whole spatial domain, and in fact we hit the numerical floor on the left side of the plot.

To see that we are converging at the expected fourth order we calculate $\log_2 |C_0|$ for each resolution, then compute the difference in successive resolutions. The resulting plot is in Fig. (5.5) and shows that indeed we are convering at fourth order on most of the domain. The odd behaviour on the left is because the higher resolution simulations have hit the numerical floor there. Further, the spikey behaviour on the right of the plot is due to the change in our finite differencing stencil as we approach the boundary. One can see this disappears as the spatial resolution is increased.

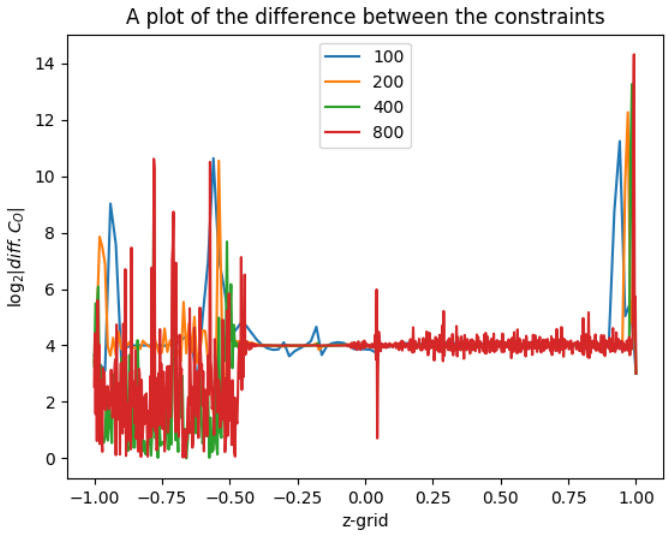

Figure 5.5: Differences between constraints for various resolutions at constant time $t = 0.4s$

5.5 Propagation of a single wave in Minkowski spacetime

As put forward in the literature review, the Minkowski spacetime forms a fundamental framework which underlies the formulation of laws of nature and their interpretation. For the same reason we explore what would arise from the propagation of a single gravitational wave in this spacetime as compared to the de Sitter spacetime. The figure below shows what was observed.

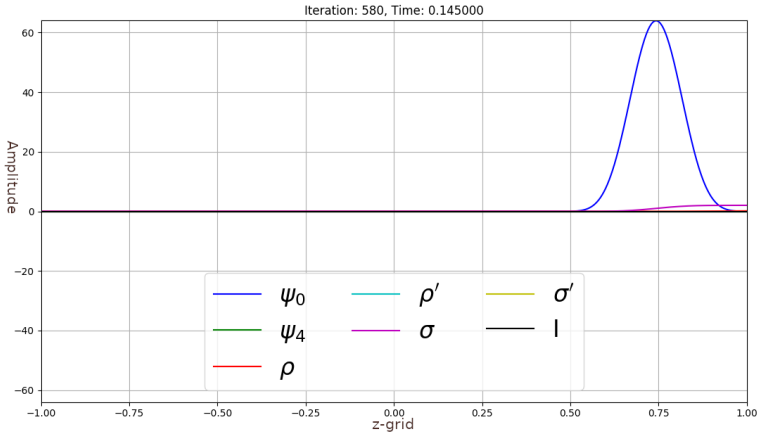

Figure 5.6: A screenshot of Ψ_0 propagating in Minkowski from the right boundary.

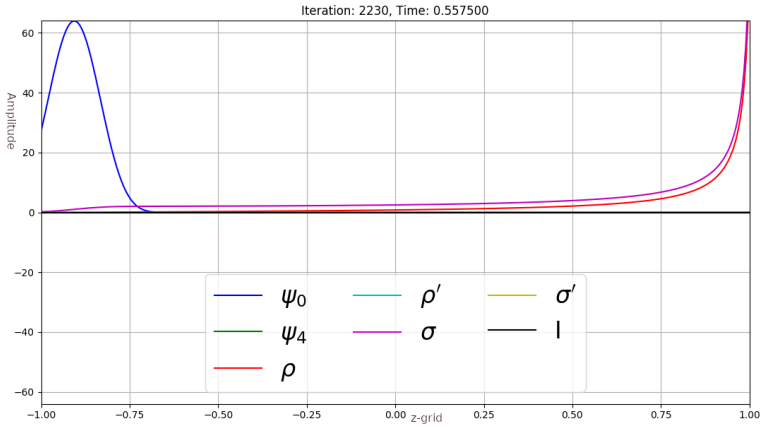

Figure 5.7: A screenshot showing the blow up of σ and ρ on the right boundary.

Fig (5.6) shows a wave front Ψ_0 propagating in from the right boundary. It then drags along a ripple effect as indicated by the σ and ρ lines which become non-zero behind the waves. Fig (5.7) then shows that after the wave passes, we notice that ρ and σ blow up on the right boundary. This is due to Sach's optical equations (5.1a) and (5.1b) put forward by Griffiths in [28] as

$$D\rho = \rho^2 + \sigma\bar{\sigma} + \Phi_{00}$$
$$D\sigma = \sigma(\rho + \bar{\rho}) + \Psi_0.$$

However, Griffiths chooses a particular gauge to arrive at these equations, whereas in our formalism, the general expressions are:

$$D\rho = \frac{1}{2}\Big(F\rho - \mu\rho + 4\rho^2 + 2\Phi_{00} + \rho\bar{F} - \rho\bar{\mu} + 2\sigma\bar{\sigma} - 2\rho\rho'\Big),$$
$$D\sigma = \frac{1}{2}\Big(3F\sigma - 3\mu\sigma + 6\rho\sigma - \sigma\bar{F} + \sigma\bar{\mu} + 2\Psi_0 - 2\sigma\rho'\Big). \tag{5.20}$$

Considering Griffiths gauge for simplicity, we note everything is initially zero. Introducing a Ψ_0 makes the RHS of the evolution equation for σ non-zero thus σ becomes non-zero. As soon as σ is non-zero, the RHS of the evolution equation for ρ becomes non-zero and so ρ becomes non-zero. The RHS of the evolution equation for ρ is strictly positive now, and thus we can say analytically that ρ will blow up which coincides with what we are observing numerically in the Friedrich-Nagy gauge.

The Kretschmann scalar with our symmetry assumptions is $I = 2\Psi_0\Psi_4 + 6\Psi_2^2$. The evolution equation for Ψ_4 tells us that it remains zero analytically. That implies that σ' and ρ' are also going to remain analytically zero. Thus $\Psi_0\Psi_4$ will always be zero. Since we have that $\Psi_2 = \sigma\sigma' - \rho\rho'$ with vanishing cosmological constant, it is also analytically zero. Therefore the Kretschmann scalar is analytically zero for all time. We find the Kretschmann scalar I is numerically zero (approximately 1e-15) for the whole evolution.

5.6 Propagation of a single wave in de Sitter spacetime

Repeating the same as above but now in the de Sitter spacetime, we show that the same analytical procedure to obtain results about the behaviour of the Kretschmann scalar and the spin-coefficients ρ and σ cannot be reproduced due to the additional complexity arising from a non-zero cosmological constant. Firstly, the introduction of a Ψ_0 causes σ to be non-zero. Then the introduction of a non-zero σ causes ρ to be non-zero, just like in the flat case. However, in this case, we also see the generation of a non-zero σ'. The non-zero σ' then causes a non-zero ρ' and Ψ_4. At which point, all system variables are non-trivial. Further, the result of the analysis for the blow up of ρ in the Minkowski case cannot be analogised due to the potential non-positivity of the RHS of the evolution equations. As for the Kretschmann scalar, because now Ψ_4 is non-zero as well

as σ' and ρ', we cannot say anything about this. This emphasises the need for a numerical analysis.

It turns out that a critical behaviour exists for one gravitational plane wave propagating in de Sitter, which is dependent on the amplitude/area of the wave packet. Thus we split our analysis into these two different situations.

5.6.1 Single wave with small amplitude

A single wave with an area of 1.4 was shoot in from the right boundary.

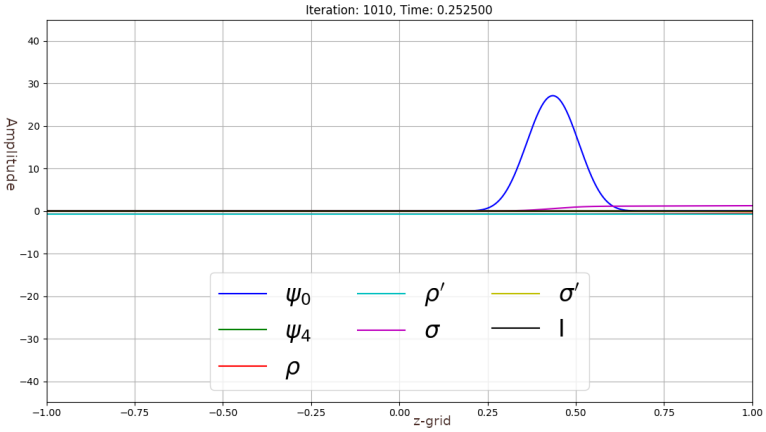

Figure 5.8: A screenshot of Ψ_0 with an area of 1.4 propagating in de Sitter after a short amount of time.

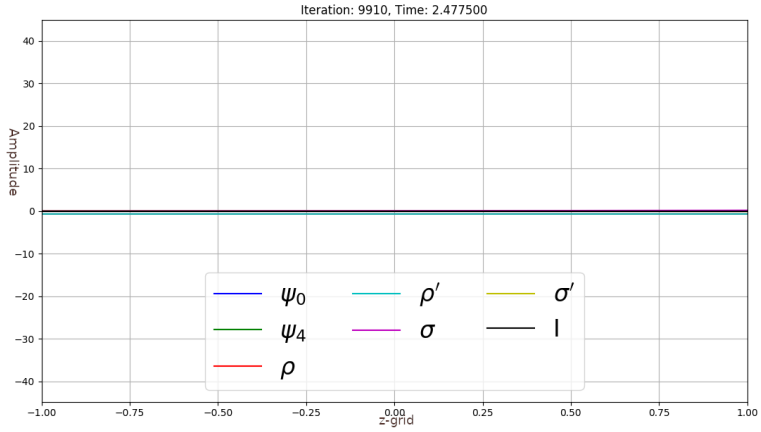

Figure 5.9: A screenshot of Ψ_0 with an area of 1.4 propagating in de Sitter after a long amount of time.

Fig (5.8) looks similar to what was observed for the Minkowski case initially, however as the space-time evolves, one sees that there is no divergent behaviour on the right boundary. Rather, the system variables all asymptote back to their initial values. A reasonable assumption to make here is that the expansion caused

by $\Lambda \neq 0$ was "too strong" for the gravitational wave, and although being contractive, gets wiped out.

5.6.2 Single wave with large amplitude

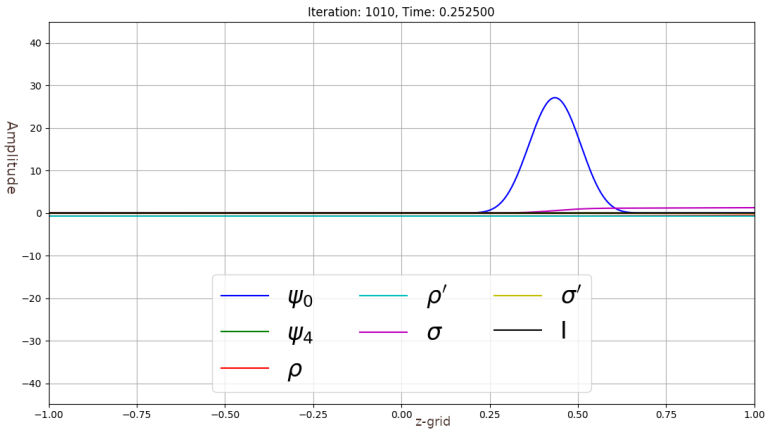

Figure 5.10: A screenshot of Ψ_0 with an area of 2 propagating in de Sitter after a short amount of time.

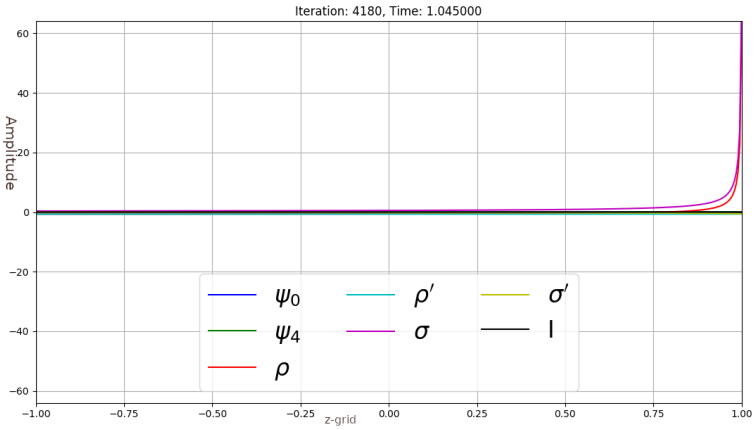

Figure 5.11: A screenshot of Ψ_0 with an area of 2 propagating in de Sitter after a long amount of time.

Initially when the wave enters the domain, we make the same initial observations as in Fig (5.8) for the previous smaller amplitude case. However sometime later, as seen in Fig (5.11), ρ and σ diverge on the right boundary, mimicking what we see in the flat case.

As the Kretschmann scalar I is non-trivial, it is interesting to see how this evolves along the right timelike boundary, see Fig. (5.12).

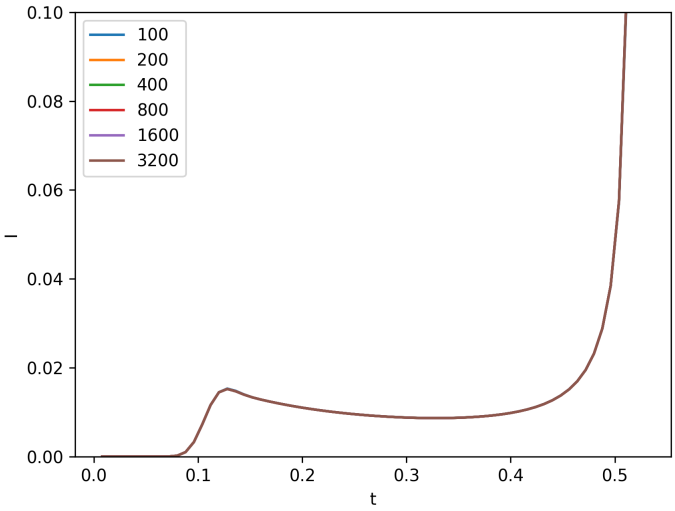

Figure 5.12: A plot of the Kretschmann scalar I from the space-time with an ingoing wave of area 3 propagating in de Sitter using multiple resolutions.

It is clear that I diverges on the boundary, but to be completely sure, we need to see how the constraints behave during this divergence. They all behave the same, and we showcase this in Fig. (5.13).

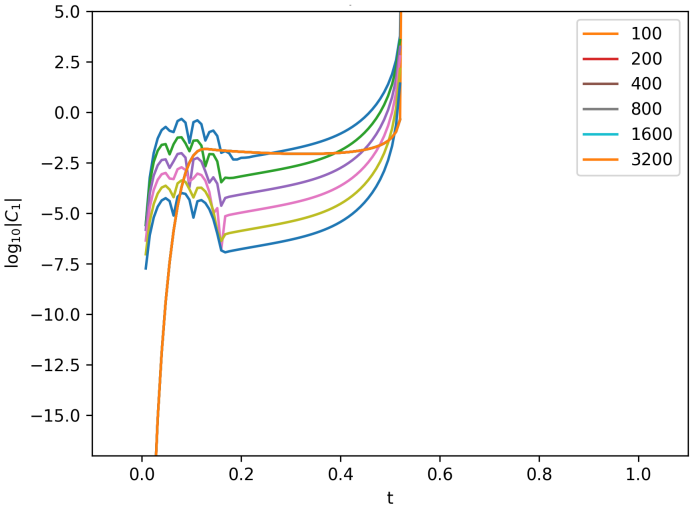

Figure 5.13: A semi-log plot of the Kretschmann scalar I from the space-time with an ingoing wave of area 3 propagating in de Sitter using multiple resolutions, overlayed with the constraint C_1.

One can see now the constraints are also diverging in time, but are definitely converging at fixed z where the Kretschmann scalar is increasing. This is good evidence to suggest we in fact do get a blow up of the Kretschmann scalar, and thus a physical curvature singularity is created. This is completely different to

Minkowski space-time equivalent, where the Kretschmann scalar is identically zero.

This section and the previous also imply that, for a fixed cosmological constant and our wave profile modulo the area, there is a critical value of the wave area that separates two distinct futures. This is no doubt caused by the relation between the strength of expansion of the space-time generated by the positive cosmological constant and the strength of contraction of the gravitational wave. This critical behaviour generates a lot of interesting properties that we now investigate further.

5.7 Critical behaviour in de Sitter spacetime

By varying the area of the wave profile for a fixed cosmological constant it was noted that there exists a critical value a_c in the sense that for values above it a future curvature singularity is formed and for values below it the spacetime will asymptote to pure de Sitter.

We are able to find these critical values to arbitrary precision by writing a simple binary search algorithm. First we find, with trial and error, two wave areas a_{low} and a_{high}, where the former causes the future space-time to asymptote to de Sitter again, and the later has a future curvature singularity. We then use this as the seed for the binary search algorithm, which will run a simulation with the wave area given by $a_{new} = (a_{low} + a_{high})/2$. If the simulation asymptotes back to de Sitter space-time within a given tolerance, then we make the replacement $a_{low} = a_{new}$. If the simulation diverges, which we can check by monitoring the size of the system variables, then we make the replacement $a_{high} = a_{new}$.

It is found that for $\Lambda = 0.5$, the critical wave area is approximately $a_c = 1.67691055$.

It is of interest to explore whether there is any special critical behaviour obtained when one is very close to this value, and whether the critical value is stable or not. For example, a rotating black hole with mass M, angular momentum J and no charge, as described by the Kerr solution, has a critical value when $J = M^2$. This value separates whether the resulting black hole has an event horizon or not.

When the exact critical value $J = M^2$ is taken, one obtains the so called extremal Kerr solution, which has properties that are different from the other two cases.

We now investigate the behaviour of our system variables, the expansion parameter H as well as the Kretschmann scalar I when we vary the area of the wave profile close to this critical value. First we look at their values along the right boundary.

5.7.1 Along the right boundary

Fig. (5.14) shows the system variables $A, B, \rho, \rho', \sigma$ and σ' plotted along the right boundary for different wave areas that are close to a_c.

Of particular interest is what happens as we take our wave profile's area closer and closer to a_c. It is clear there is a period of time, roughly in the interval $[3, 7]$ for the simulations whose wave area is closest to a_c, where these variables become constant. The closer we get to the critical value, the longer this constant interval becomes. This gives evidence for the critical value being an unstable one, and that there may be a new solution, constant in time, which has different values to the initial data.

Some notes regarding the behaviour of individual system variables:

The A and B variables dictate the scales in the t and z directions, and these plots show that for wave areas taken less than a_c, the z-directions become more and more stretched, as they return to their initial values describing an expanding universe. For waves with larger area than a_c, the resulting B will approach $+1$, causing the z coordinate vector to become null and thus crash the simulation.

The ρ and ρ' variables both start negative, describing a diverging null congruence in both ingoing and outgoing null directions. However for waves with area greater than a_c, we see that both of these diverge toward $+\infty$, showing that these congruences become contractive. This indicates the presence of a singularity at some time in the future, which by noting our analysis of the Kretschmann scalar as seen in Fig (5.13), we can say is a physical one.

Now also noting Fig. (5.15), we see that all ρ', σ', ψ_4 and I are non-zero, in stark contrast to the Minkowski case. The ψ_4 is generated (eventually) by the

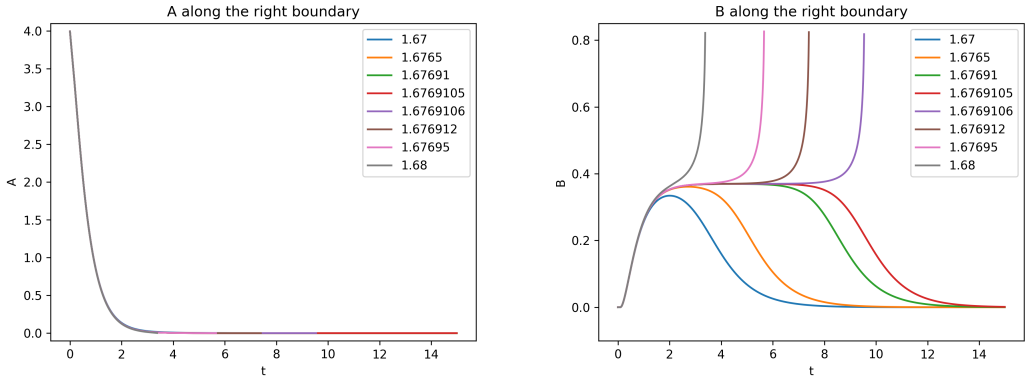

(a) A

(b) B

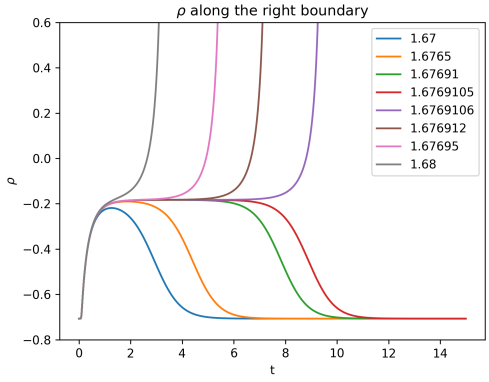

(c) ρ

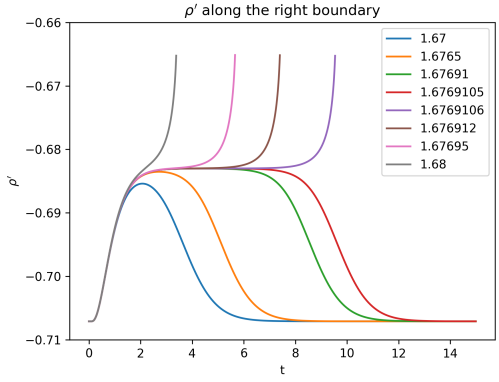

(d) ρ'

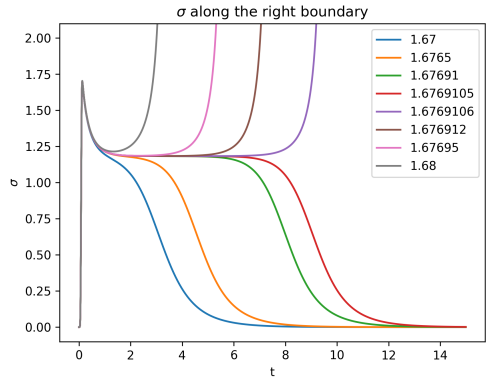

(e) σ

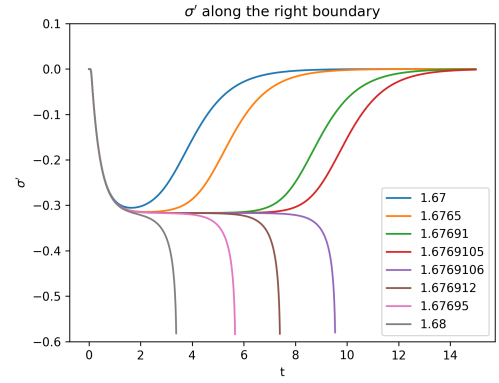

(f) σ'

Figure 5.14: Plots of the system variables $A, B, \rho, \rho', \sigma, \sigma'$ along the right boundary over time for different wave areas close to the critical value.

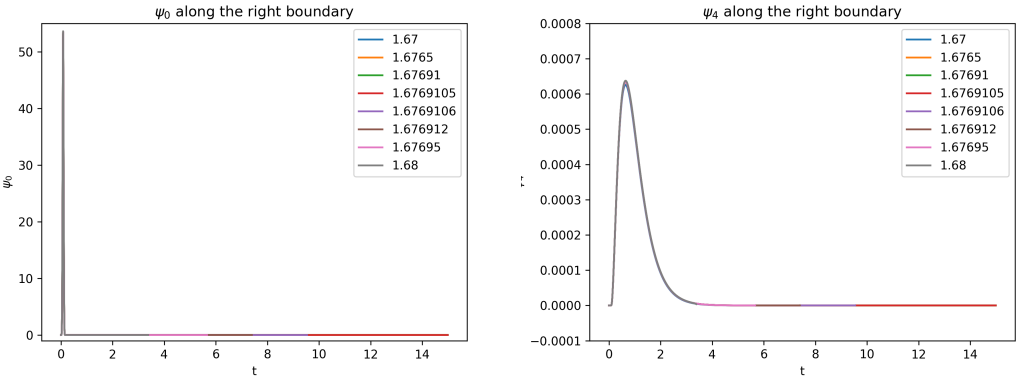

(a) ψ_0

(b) ψ_4

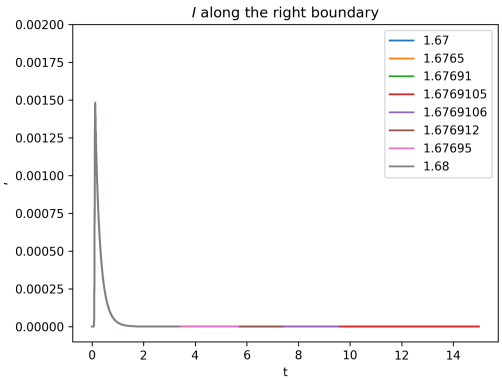

(c) I

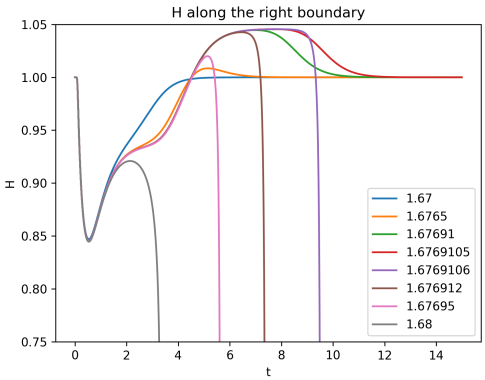

(d) H

Figure 5.15: Plots of the system variables ψ_0, ψ_4, the Kretschmann scalar I and our expansion parameter H along the right boundary over time for different wave areas close to the critical value.

presence of a non-vanishing ψ_0, which indicates that the presence of a positive cosmological constant allows for a non-linear back-reaction to occur. The non-vanishing of ρ' and σ' indicates that there is a convergence/divergence and a shear in a congruence of outgoing null geodesics emanating from the boundary, which is expected with a non-vanishing outgoing wave.

It is interesting to note that the Kretschmann scalar I as well as other spin coefficients do not blow up for supercritical wave areas but rather asymptote to their original values. This is a new type of singularity admitted by our gauge caused by the divergence of μ to $+\infty$.

Finally, looking at our expansion parameter H we see that it is initially one, but decreases shortly after. This is due to the attractive nature of gravity and hence of our wave. The simulations with the larger wave areas eventually show that H diverges toward $-\infty$, which indicates the space-time slows down its expansion and eventually reverses this into a contraction, in accordance with what we have already concluded about the existence of a future curvature singularity. For waves with an area less than a_c we find the interesting property that the expansion parameter actually gets larger than the original value of 1 for a short time, before asymptoting back to it's original value. Like in all the other variables, we see that there is a period at which H becomes constant. If we are to believe that there does exist a critical solution, where our variables, except A, are constant in time, with different constant values to the initial ones, then it is very interesting that the expansion parameter is *larger* than the initial value. This of course indicates that the critical solution would be expanding at a faster rate.

5.7.2 On an entire timeslice

As we have only seen what is happening along the boundary where the wave is propagated in from, the next step is to see the what the variables are doing on an entire timeslice.

A selection of system variables on a timeslice during the constant period, at $t = 6.02$, over the whole spatial grid are displayed in Fig. (5.16). Firstly, one notices that the small differences in wave area between simulations only affects the variables within the accuracy of the plotted curve. Importantly, one sees it is

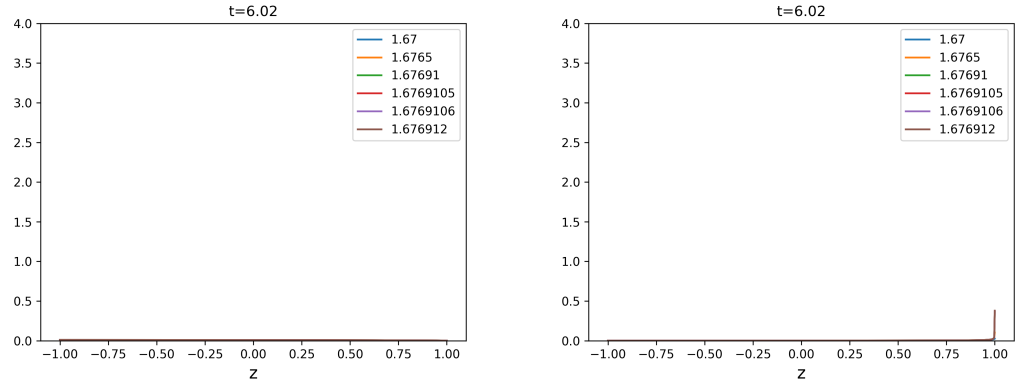

(a) A

(b) B

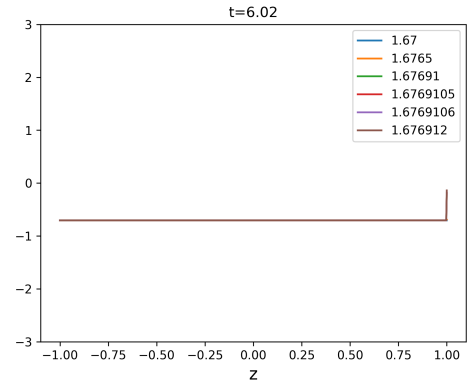

(c) ρ

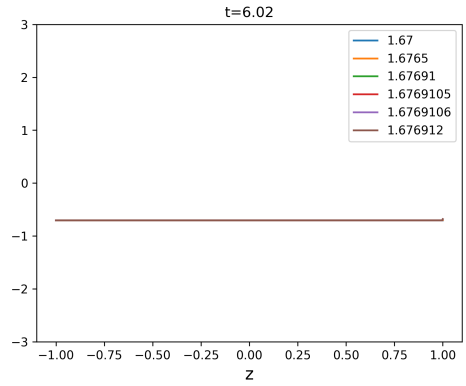

(d) ρ'

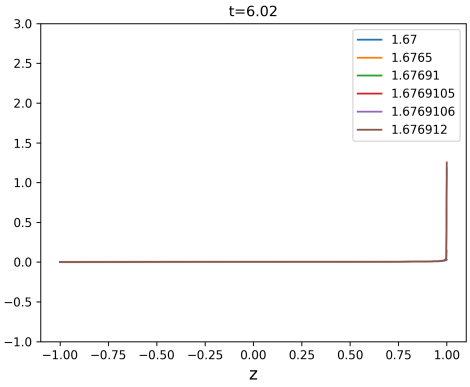

(e) σ

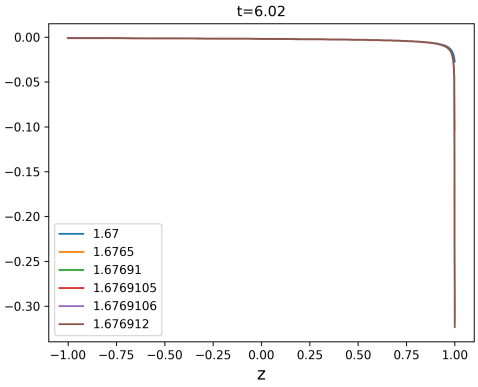

(f) σ'

Figure 5.16: Plots of the system variables $A, B, \rho, \rho', \sigma, \sigma'$ on the timeslice $t = 6.02$ for different wave areas close to the critical value.

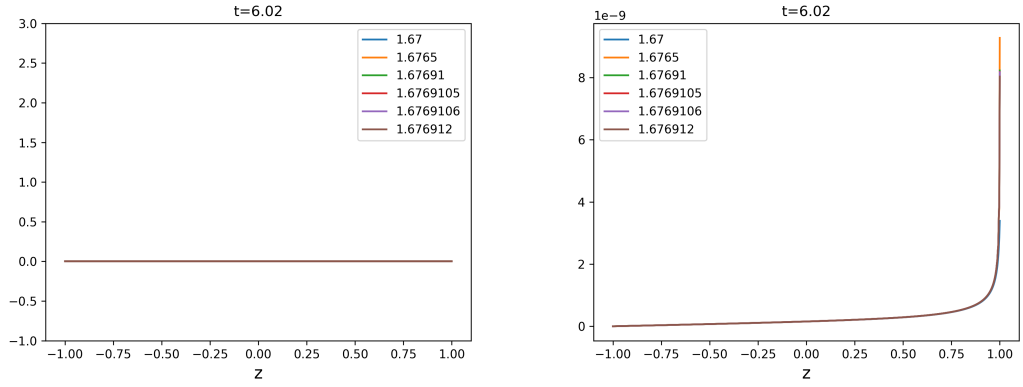

(a) ψ_0

(b) ψ_4

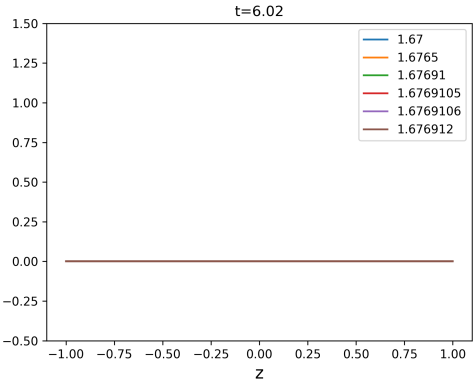

(c) I

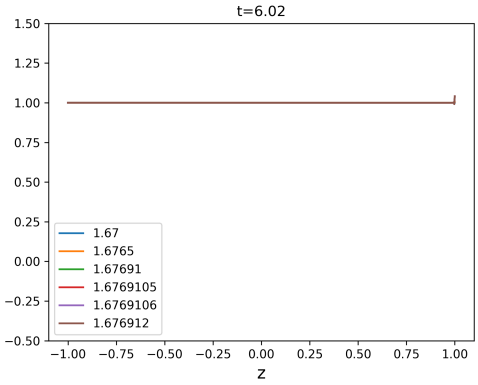

(d) H

Figure 5.17: Plots of the system variables ψ_0, ψ_4, the Kretschmann scalar I and our expansion parameter H on the timeslice $t = 6.02$ for different wave areas close to the critical value.

only the values of the system variables *on the boundary* that are exhibiting a short phase whereby they are roughly constant in time. Everywhere else the variables seem to be settling back to their initial values, except the cases where the area of the wave profile was greater than a_c, which diverge on the right boundary instead.

In Fig. (5.17) we see ψ_0, ψ_4, I and H plotted over the timeslice. These all exhibit the same behaviour as the other variables plotted in Fig. (5.16), namely they asymptote back to their original values in the interior, and either do the same on the right boundary or diverge depending on whether the wave area is smaller or larger than a_c.

5.7.3 Critical wave areas for different Λ

It is useful to plot quantities with respect to a single dimensionless quantity which may be scale invariant. Dimensionless quantities are found as ratios of quantities having dimensions, in our case we only have l = length. In our case,

the two quantities we have available are Λ, which has dimension l^{-2} and the parameters of our wave such as the area, which has dimension l^3. If we could find a dimensionless quantity, say $D = D(a_c, \Lambda)$, which is a *constant*, this could then be used as a simple way to, given a fixed Λ, obtain the critical wave area without a time consuming binary search being performed.

To calculate the area of our wave profile on the boundary, note that the metric tensor can be expressed as $g_{ab} = g_{ij}(dx^i)_a(dx^j)_a$, where g_{ab} is abstract and g_{ij} are the components in the $\mathrm{d}x^i$ basis. As g_{ab} has dimension l^2, we take the convention that g_{ij} is dimensionless and the dx^i have dimension length. This then implies that Ψ_0 has dimension l^2 and a_c has dimension l^3.

Thus the simplest possible dimensionless quantity we could define from these is $D_1 := \Lambda^3/a_c^2$, which we plot in Fig. (5.18). The quantity is clear not constant and increases with time.

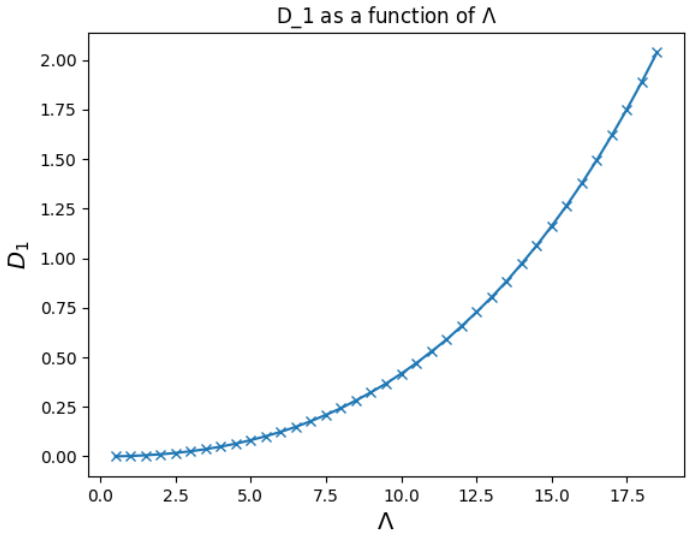

Figure 5.18: A plot of the dimensionless quantity $D_1 := \Lambda^3/a_c^2$.

Another possibility could be to use the Bel-Robinson notion of energy. In spinor notation, the Bel-Robinson tensor is defined as [41]

$$T_{AA'BB'CC'DD'} := \Psi_{ABCD}\overline{\Psi}_{A'B'C'D'}. \tag{5.21}$$

Transvecting this with the timelike vector $t^a = (l^a + n^a)/\sqrt{2}$, and recalling $\Psi_1 = 0 = \Psi_3$, we define

$$\begin{aligned} E_{BR} &:= \int_{t_0}^{t_1} t^{AA'} t^{BB'} t^{CC'} t^{DD'} \Psi_{ABCD} \bar{\Psi}_{A'B'C'D'} \mathrm{d}t \\ &= \frac{1}{4} \int_{t_0}^{t_1} (\Psi_0 \bar{\Psi}_0 + 6\Psi_2 \bar{\Psi}_2 + \Psi_4 \bar{\Psi}_4) \mathrm{d}t, \end{aligned} \tag{5.22}$$

where the bounds cover the wave profile on the boundary. From the above analysis, this has dimensions l^5. Thus we can create another dimensionless quantity, $D_2 := \Lambda^5 / {E_{BR}}^2$, shown in Fig. (5.19). This looks similar to the plot of D_1.

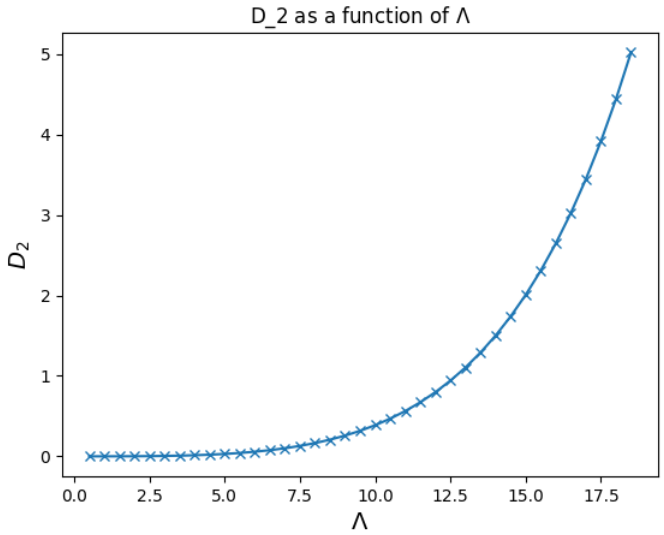

Figure 5.19: A plot of the dimensionless quantity $D_2 := \Lambda^5 / {E_{BR}}^2$.

It turns out that these two dimensionless quantities, although not constant, may follow a power-law. This is found by looking at a log-log plot, shown in Fig. (5.20), where the line of best fit is overlaid. We have the linear approximations

$$\log(D_1) \approx -6.1014 + 2.2897 \log(\Lambda) \Rightarrow D_1 \approx 0.00224 \Lambda^{2.2897}, \tag{5.23}$$

$$\log(D_2) \approx -9.1139 + 3.5845 \log(\Lambda) \Rightarrow D_2 \approx 0.00011 \Lambda^{3.5845}. \tag{5.24}$$

One can see a pretty good fit for the data we have, but it requires a larger data set to really see if this relationship holds for a larger range of critical values.

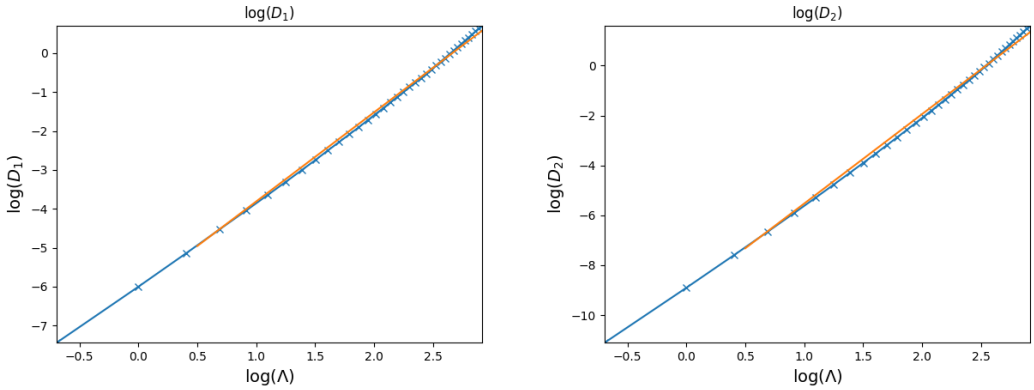

(a) $\log(D_1)$ (b) $\log(D_2)$

Figure 5.20: Log-log plots of D_1 and D_2 with a linear best fit overlaid.

Chapter 6

Conclusions

In this research we investigated the evolution of plane gravitational waves in de Sitter space-time numerically which were analogised with the Minkowski case. We implemented the equations in the Newman-Penrose formalism together with the Friedrich-Nagy gauge [26], closely following [24]. This gave us a wellposed IBVP to use for our numerical evolutions.

The space-time was evolved numerically using COFFEE [20], an already developed `Python` package for the numerical solution of PDEs using the method of lines. We used Strand's finite difference operator with the summation-by-parts property [46] for approximating the spatial derivatives, explicit Runga-Kutta 4 for evolving in time and the simultaneous-approximation-term method [13] for imposing stable boundary conditions.

We first numerically reproduced known analytical results concerning the propagation of a single wave from the right boundary on Minkowski space-time, which has a vanishing cosmological constant. In accordance with these analytical results, we numerically found that the divergence spin-coefficient in the l^a direction, ρ, would blow up on the boundary the wave was introduced as the RHS of its evolution equation became strictly increasing due to the introduction of a Ψ_0. The Kretschmann scalar I, a scalar curvature invariant, was identically zero. These results were then used as a basis for discussions of what was observed for the de Sitter case.

It was discovered that a wave front with a small enough area propagating in de Sitter space-time with a positive cosmological constant did not cause any spin-coefficients to diverge. This was explained due to the accelerated expansion wiping the wave out and allowing the space-time to asymptote back to pure

de Sitter, thus showing a completely different phenomenon as compared to the Minkowski case. The case of a wave with a large enough area propagating in de Sitter was then considered. It was revealed that in this situation ρ diverges at the right boundary, which was different to what was observed for the smaller area case. Thus, there exists some critical wave area a_c such that waves with an area below this value the future space-time will asymptote to pure de Sitter, while for values above a future singularity will occur. For $\lambda = 0.5$, the critical wave area a_c, obtained by performing a binary search, was found to be approximately 1.67691055.

An investigation into the behavior of the system variables was then carried out by varying the wave profile areas close to a_c. It was noted that waves whose areas were closer to a_c took longer to either blow up or asymptote to de Sitter, and in the meantime took on a constant value in time on the right boundary different from their initial values. This led us to conclude the possibility of the existence of a new solution, obtained by taking the exact critical value. It is clear this critical value is unstable and thus this cannot be fully realised numerically. In the cases where a future singularity occurs, we presented evidence of this being a curvature singularity by closely analysing the behaviour of the Kretschmann scalar. The expansion parameter H revealed that gravitational radiation does affect the expansion of the universe in a contractive way. For wave areas smaller than a_c, our H initially decreases but then interestingly increases to a value slightly above the initial value of $H = 1$, before either settling back down to 1 or diverging to $-\infty$.

We also looked at the system variables over the whole spatial domain at a constant time. This showed that everywhere except the right boundary, the system asymptotes back to its initial state. This shows that the most complicated behaviour is happening on the right boundary.

Finally, we investigated the critical wave area a_c for a set of different λ. We presented two dimensionless quantities made up of a_c and λ, to try and see if a simple relationship existed, such as $f(\lambda, a_c) = \text{constant}$. The closest we could find was that a power law would be the best fit.

6.1 Future work

In this research we investigated the case of a single wave propagating in de Sitter space time and so considering the case of two colliding gravitational waves with the same polarisation would be intriguing. This case was never explored before as proved in the existing literature. This possible future work could be achieved by making use of the same COFFEE package made use of in this research. Interesting phenomena can be found for this case in the interaction region for instance the formation of a trapped surface.

More so, we only considered the propagation of a single wave profile and it was revealed that the expansion rate was greatly affected. Hence, having a look at the propagation of a continuous stream of waves from one boundary with areas close to the critical value a_c and see if expansion will be halted will be interesting. Moreover, it could be fascinating to look into the collision of such continuous streams of waves and analyse any interesting phenomena.

The case investigated involved a single wave profile and therefore a look at a single wave with a different polarisation could be interesting, and is accomplished by multiplying the wave profile by a phase. This could be extended to the case of two colliding waves with different polarisations.

It has recently been shown that, from an analytic point of view, data induced on the null hypersurfaces $u = 0 = v$ from two colliding gravitational plane waves with the initial region being Minkowskian, can lead to a solution of the Einstein equations in the interaction region with a positive cosmological constant. It could be interesting to investigate this numerically by adding some mechanism to turn on the cosmological constant, such as a scalar field.

Bibliography

[1] B. Abbott, R. Abbott, T. Abbott, S. Abraham, F. Acernese, K. Ackley, C. Adams, R. Adhikari, V. Adya, C. Affeldt *et al.*, 'Gwtc-1: A gravitational-wave transient catalog of compact binary mergers observed by ligo and virgo during the first and second observing runs', *Physical Review X*, vol. 9, no. 3, p. 031 040, 2019.

[2] S. Abraham, T. Abbott, R. Abbott, F. Acernese, K. Ackley, A. Adams, C. Adams, R. Adhikari, V. Adya, C. Affeldt *et al.*, 'Gwtc-2: Compact binary coalescences observed by ligo and virgo during the first half of the third observing run', *arXiv preprint arXiv:2010.14527*, 2020.

[3] M. Alcubierre, *Introduction to 3+ 1 numerical relativity*. Oxford University Press, 2008, vol. 140.

[4] F. Beyer, B. Daszuta, J. Frauendiener and B. Whale, 'Numerical evolutions of fields on the 2-sphere using a spectral method based on spin-weighted spherical harmonics', *Classical and Quantum Gravity*, vol. 31, no. 7, p. 075 019, 2014.

[5] F. Beyer, G. Doulis, J. Frauendiener and B. Whale, 'Linearized gravitational waves near space-like and null infinity', in *Progress in Mathematical Relativity, Gravitation and Cosmology*, Springer, 2014, pp. 3–17.

[6] F. Beyer, G. Doulis, J. Frauendiener and B. Whale, 'The spin-2 equation on minkowski background', in *Progress in Mathematical Relativity, Gravitation and Cosmology*, Springer, 2014, pp. 465–468.

[7] F. Beyer, G. Doulis, J. Frauendiener and B. Whale, 'Numerical space-times near space-like and null infinity. the spin-2 system on minkowski space', *Classical and Quantum Gravity*, vol. 29, no. 24, p. 245 013, 2012.

[8] F. Beyer, J. Frauendiener, C. Stevens and B. Whale, 'Numerical initial boundary value problem for the generalized conformal field equations', *Physical Review D*, vol. 96, no. 8, p. 084 020, 2017.

[9] J. Bičák and J. Podolskỳ, 'Gravitational waves in vacuum spacetimes with cosmological constant. i. classification and geometrical properties of nontwisting type n solutions', *Journal of Mathematical Physics*, vol. 40, no. 9, pp. 4495–4505, 1999.

[10] J. Bičák and J. Podolskỳ, 'Gravitational waves in vacuum spacetimes with cosmological constant. ii. deviation of geodesics and interpretation of nontwisting type n solutions', *Journal of Mathematical Physics*, vol. 40, no. 9, pp. 4506–4517, 1999.

[11] H. Bondi and F. Pirani, 'Gravitational waves in general relativity-xiii. caustic property of plane waves', *Proceedings of the Royal Society of London. A. Mathematical and Physical Sciences*, vol. 421, no. 1861, pp. 395–410, 1989.

[12] H. Bondi, F. A. Pirani and I. Robinson, 'Gravitational waves in general relativity iii. exact plane waves', *Proceedings of the Royal Society of London. Series A. Mathematical and Physical Sciences*, vol. 251, no. 1267, pp. 519–533, 1959.

[13] M. H. Carpenter, D. Gottlieb and S. Abarbanel, 'The stability of numerical boundary treatments for compact high-order finite-difference schemes', *Journal of Computational Physics*, vol. 108(2):272-295, 1993.

[14] J. L. Cervantes-Cota, S. Galindo-Uribarri and G. F. Smoot, 'A brief history of gravitational waves', *Universe*, vol. 2, no. 3, p. 22, 2016.

[15] G. B. Cook, 'Initial data for numerical relativity', *Living reviews in relativity*, vol. 3, no. 1, pp. 1–53, 2000.

[16] R. Courant, K. Friedrichs and H. Lewy, ' "U on the partial difference equations of mathematical physics', *mathematical annals*, vol. 100, no. 1, pp. 32–74, 1928.

[17] W. Dewi and Triyanta, 'Gravitational waves in minkowski spacetime background', *Journal of Physics: Conference Series*, vol. 1428, p. 012 058, Jan. 2020. DOI: 10.1088/1742-6596/1428/1/012058. [Online]. Available: https://doi.org/10.1088/1742-6596/1428/1/012058.

[18] P. Diener, E. N. Dorband, E. Schnetter and M. Tiglio, 'Optimized high-order deriva- tive and dissipation operators satisfying summation by parts, and applications in three-dimensional multi-block evolutions', *Journal of Scientific Computing*, vol. 32(1):109– 145, 2007.

[19] A. Dominguez and F. Prada, 'Measurement of the expansion rate of the universe from γ-ray attenuation', *The Astrophysical Journal Letters*, vol. 771, no. 2, 2013.

[20] G. Doulis, J. Frauendiener, C. Stevens and B. Whale, 'Coffee – an mpi-parallelized python package for the numerical evolution of differential equations', *SoftwareX*, vol. 10, 2019. arXiv: 1903.12482 [cs.MS]. [Online]. Available: http://www.sciencedirect.com/science/article/pii/S2352711019300950.

[21] G. Doulis and J. Frauendiener, 'The second order spin-2 system in flat space near space-like and null-infinity', *General Relativity and Gravitation*, vol. 45, no. 7, pp. 1365–1385, 2013.

[22] G. Doulis and J. Frauendiener, 'Global simulations of minkowski spacetime including spacelike infinity', *Physical Review D*, vol. 95, no. 2, p. 024 035, 2017.

[23] J. Ehlers and W. Kundt, 'Exact solutions of the gravitational field equations', in *The Theory of Gravitation*, John Wiley & Sons, Inc., 1962, pp. 49–101.

[24] J. Frauendiener, C. Stevens and B. Whale, 'Numerical evolution of plane gravitational in the friedrich-nagy gauge', *Physical Review D*, vol. 90, 2014.

[25] H. Friedrich, 'Einstein equations and conformal structure: Existence of anti-de sitter-type space-times', *Journal of Geometry and Physics*, vol. 17, no. 2, pp. 125–184, 1995. DOI: https://doi.org/10.1016/0393-0440(94)00042-3.

[26] H. Friedrich and G. Nagy, 'The initial boundary value problem for einstein's vacuum field equation', *Communications in Mathematical Physics*, vol. 201, pp. 619–655, 1999.

[27] J. Gong and J. Nordström, 'Interface procedures for finite difference approximations of the advection–diffusion equation', *Journal of Computational and Applied Mathematics*, vol. 236(5):602–620, 2011.

[28] J. B. Griffiths, *Colliding plane waves in general relativity*. Oxford, Oxford University Press, 1991, vol. 1.

[29] S. W. Hawking and G. F. R. Ellis, *The large scale structure of space-time*. Cambridge university press, 1973, vol. 1.

[30] E. Hubble, 'A relation between distance and radial velocity among extra-galactic nebulae', *Proceedings of the national academy of sciences*, vol. 15, no. 3, pp. 168–173, 1929.

[31] K. A. Khan and R. Penrose, 'Scattering of two impulsive gravitational waves', *Nature*, vol. 229, 1971.

[32] H. O. Kreiss and O. E. Ortiz, *Some mathematical and numerical questions connected with first and second order time-dependent systems of partial differential equations*. Springer, Berlin, Heidelberg, 2002, pp. 359–370.

[33] K. Mattsson and J. Nordström, 'Summation by parts operators for finite difference approximations of second derivatives', *Journal of Computational Physics*, vol. 199, no. 2, pp. 503–540, 2004.

[34] E. T. Newman and R. Penrose, 'An approach to gravitational radiation by a method of spin coefficients', *Journal of Mathematical Physics*, vol. 3(3):566–578, 1962.

[35] E. T. Newman and R. Penrose, 'Spin-coefficient formalism', *Scholarpedia*, vol. 4, no. 6, p. 7445, 2009, revision #184895. DOI: 10.4249/scholarpedia.7445.

[36] Y. Nutku and M. Halil, 'Colliding impulsive gravitational waves', *Physical Review Letters*, vol. 39, no. 22, p. 1379, 1977.

[37] D. Overbye, 'Cosmos controversy: The universe is expanding, but how fast?', *The New York Times*, vol. 20, 2017.

[38] R. Penrose, 'A spinor approach to general relativity', *Annals of Physics*, vol. 10(2):171–201, 1960.

[39] R. Penrose and W. Rindler, *Spinors and Spacetime: Two-Spinor Calculus and Relativistic Fields*. Cambridge University Press, Cambridge, England, 1984, vol. 1.

[40] R. Penrose, 'A remarkable property of plane waves in general relativity', *Reviews of Modern Physics*, vol. 37, no. 1, p. 215, 1965.

[41] R. Penrose, 'Twistor quantisation and curved space-time', *International Journal of Theoretical Physics*, vol. 1, no. 1, pp. 61–99, 1968.

[42] J. Podolskỳ and K. Veselỳ, 'New examples of sandwich gravitational waves and their impulsive limit', *Czechoslovak journal of physics*, vol. 48, no. 8, pp. 871–878, 1998.

[43] J. Podolskỳ, C. Sämann, R. Steinbauer and R. Švarc, 'Cut-and-paste for impulsive gravitational waves with Λ: The geometric picture', *Physical Review D*, vol. 100, no. 2, p. 024 040, 2019.

[44] B. F. Schutz, 'Gravitational radiation', *arXiv preprint gr-qc/0003069*, 2000.

[45] S. Singh, *The Origin of the Universe*. Harper Perennial, 2005.

[46] B. Strand, 'Summation by parts for finite difference approximations for d/dx', *Journal of Computational Physics*, vol. 110, no. 1, pp. 47–67, 1994.

[47] N. Tsamis and R. Woodard, 'Pure gravitational back-reaction observables', *Physical Review D*, vol. 88, no. 4, 2013.

[48] N. Tsamis and R. Woodard, 'Classical gravitational back-reaction', *Classical and Quantum Gravity*, vol. 31, no. 18, p. 185 014, 2014.

[49] R. M. Wald, *General relativity*. University of Chicago Press, Chicago, London, 1984, vol. 1.

[50] Wikipedia contributors, *First observation of gravitational waves — Wikipedia, the free encyclopedia*, [Online; accessed 18-February-2021], 2021. [Online]. Available: `https://en.wikipedia.org/w/index.php?title=First_observation_of_gravitational_waves&oldid=998970140`.

[51] Wikipedia contributors, *Pp-wave spacetime — Wikipedia, the free encyclopedia*, [Online; accessed 17-February-2021], 2021. [Online]. Available: `https://en.wikipedia.org/w/index.php?title=Pp-wave_spacetime&oldid=1000149021`.

Appendix A

Important concepts

In this section building blocks necessary for the derivation of the field equations are laid and we closely follow the definitions put forward by Wald in [49].

A.1 Manifolds

Wald [49] defines an n-dimensional infinitely continuously differentiable, C^∞, real manifold M as a set together with a collection of subsets $\{O_\alpha\}$ satisfying the following properties:

• The subsets $\{O_\alpha\}$ cover M, that is every $p \in M$ lies in at least one O_α.

• For each α, there is an onto map or coordinate system $\psi_\alpha : O_\alpha \to U_\alpha$, where U_α is an open subset of ^{n}.

• If any two sets $O_\alpha$and O_β overlap, then $O_\alpha \cap O_\beta \neq \emptyset$ and we can consider the map $\psi_\beta \circ {\psi_\alpha}^{-1}$ to be C^∞ since the maps are of $\mathbb{R}^n$ into $\mathbb{R}^n$.

A.1.1 Tangent vectors and co-vectors

On a manifold M, let Ξ denote a collection of C^∞ functions from M to $\mathbb{R}$. We can then define a **tangent vector** v at a point $p \in M$ as a map $v : \Xi \to \mathbb{R}$ which is linear and obeys the following Leibnitz rule

$$\bullet\, v(af + bg) = av(f) + bv(g), \forall f, g \in \Xi; a, b \in \mathbb{R}$$

$$\bullet\, v(fg) = f(p)v(g) + g(p)v(f)$$

Thus a tangent vector is a directional derivative operator acting on a collection of functions defined on a manifold M that is, if x^μ is a curve, parametrised by s

such that $x^\mu = x^\mu(s)$, living on M then the components of a tangent vector at any point depending on the coordinates are given by

$$V^\mu = \frac{dx^\mu(s)}{ds}.$$

Likewise if given a function g and a curve on a manifold parametrised by s then the directional derivative at a point p on the curve is defined as

$$\frac{dg}{ds}|_p = \frac{dx^\mu}{ds}|_p \frac{\partial g}{\partial x^\mu},$$

drop the arbitrary function g, the directional derivative at p can then be written as

$$\mathbf{V}_p = \frac{d}{ds}|_p = \frac{dx^\mu}{ds}|\frac{\partial}{\partial x^\mu} = \frac{dx^\mu}{ds}\partial_\mu$$

From this definition it is easy to note that a collection of tangent vectors at a point is a vector space also known as the tangent space T_p of the manifold.
A **co-vector** can be defined as an object that maps a vector to a number and is given by

$$\omega = \omega_\mu dx^\mu$$

The action of such a co-vector on a vector $V = V^\nu \partial_\nu$ can be written as

$$\omega(V) = \omega_\mu dx^\mu V^\nu \partial_\nu = \omega_\mu V^\mu$$

and similarly a collection of co-vectors at a point p form a co-tangent space T_{*p} to the manifold.

A.1.2 Covariant derivative

The covariant derivative, ∇, sometimes called the derivative operator on a manifold M is defined as a map which takes each smooth tensor field of type (k, l) to a smooth tensor field of type $(k, l+1)$ thus it gives the rate of change of a tensor. For two vector fields $\mathbf{w}$ and $\mathbf{x}$ and any tensors $\mathbf{Y}$ and $\mathbf{Z}$, the covariant derivative has the following properties

• Linearity: $\forall \alpha, \beta \in \mathbb{R}$

$$\nabla_{\mathbf{x}}(\alpha\mathbf{Y} + \beta\mathbf{Z}) = \alpha\nabla_{\mathbf{x}}\mathbf{Y} + \beta\nabla_{\mathbf{x}}\mathbf{Z}$$

• Leibnitz rule:

$$\nabla_{\mathbf{x}}[\mathbf{Y}\otimes\mathbf{Z}] = [\nabla_{\mathbf{x}}\mathbf{Y}]\otimes\mathbf{Z} + \mathbf{Y}\otimes[\nabla_{\mathbf{x}}\mathbf{Z}]$$

• Additiveness: For functions f and g,

$$\nabla_{\mathbf{x}f+\mathbf{w}g}\mathbf{Z} = f\nabla_{\mathbf{x}}\mathbf{Z} + g\nabla_{\mathbf{w}}\mathbf{Z}$$

• Action on scalar: For a scalar α,

$$\nabla_{\mathbf{x}}(\alpha) = X(\alpha)$$

• Action on a vector: In component form, for a vector A^λ,

$$\nabla_\nu A^\lambda = \partial_\nu A^\lambda + \Gamma^\lambda{}_{\mu\nu}A^\mu$$

where $\Gamma^\lambda{}_{\mu\nu}$ is the connection defined in the following section.

A.1.3 Connection and geodesic equation

The connection, $\Gamma^\lambda{}_{\mu\nu}$, is an object that is used to compare vectors in different tangent spaces, i.e it connects tangent spaces. It is symmetric in its lower indices and is metric compatible. This definition leads directly to the identity

$$\nabla_\sigma(g_{\mu\nu}) \equiv 0 \tag{A.1}$$

From this identity, the connection can now be expressed as (see proof in the Appendix)

$$\Gamma^\lambda{}_{\mu\nu} = \frac{1}{2}g^{\lambda\sigma}(\partial_\mu g_{\mu\sigma} + \partial_\nu g_{\nu\sigma} - \partial_\sigma g_{\mu\nu}).$$

The connection is also very useful in the definition of geodesics. These geodesics are solutions to the geodesic equation given by auto parallel curves

$$U^\mu\nabla_\mu U^\nu = kU^\nu \quad \Leftrightarrow \quad \frac{\mathbf{d}^2x^\rho}{\mathbf{d}s^2} + \Gamma^\rho{}_{\nu\sigma}\frac{\mathbf{d}x^\nu}{ds}\frac{\mathbf{d}x^\sigma}{ds} = 0$$

A.1.4 Killing vectors

Previously we defined the notion of vectors that act on curves that exist on manifolds. We have since introduced more objects, these being tensors, that exist on a manifold. It makes sense then that we must have object that will act on tensors much like vectors on curves.

We then define the Lie derivative, $\pounds_v$, which is a linear map from (k,l) tensor

fields to (k,l) tensor fields along a vector v . Like the covariant derivatives, the Lie derivative obeys Leibnitz rule. For a general tensor field, $T^{\mu_1\cdots\mu_k}{}_{\nu_1\ldots\nu_l}$, and vector fields v^μ, v^σ it can be shown by induction that for any covariant derivative operator ∇_μ

$$\begin{aligned}\pounds_v T^{\mu_1\cdots\mu_k}{}_{\nu_1\ldots\nu_l} &= v^\sigma \nabla_\sigma T^{\mu_1\cdots\mu_k}{}_{\nu_1\ldots\nu_l} - \sum_{i=1}^{k} T^{\mu_1\ldots\sigma\ldots\mu_k}{}_{\nu_1\ldots\nu_l}\nabla_\sigma v^{\mu_i} \\ &+ \sum_{j=1}^{l} T^{\mu_1\cdots\mu_k}{}_{\nu_1\ldots\sigma\ldots\nu_l}\nabla_{\nu_j} v^\sigma.\end{aligned}$$

When the Lie derivative operates on the metric tensor, $g_{\mu\nu}$, that is using the above definition, we obtain a useful Killing equation

$$\pounds_v g_{\mu\nu} = 2\nabla_{(\mu}V_{\nu)}.$$

Any vector that preserves the metric, i.e

$$\pounds_v g_{\mu\nu} = 0 \quad \Rightarrow \nabla_{(\mu}V_{\nu)} = 0$$

is known as a *Killing vector*. As discussed in section (3.1.12), the existence of Killing vectors is vital when solving Einstein's field equations as they add symmetries and enable us solve complex equations easily.

A.2 Tensor

The formalism most commonly used for the treatment of manifolds and their metrics is tensor calculus [39]. A tensor T of type (k,l) at a point p is defined as a multilinear map from k copies of a co-tangent space and l copies of a tangent space to produce a real number.

$$T = T^{\mu_1\mu_2\cdots\mu_k}{}_{\nu_1\nu_2\ldots\nu_l}\partial_{\mu_1}\ldots\partial_{\mu_k}dx^{\nu_1\nu_2\ldots\nu_l}$$

In studying the laws of physics in the context of curved spacetime, many tensors are used and the important ones to this research are defined below.

A.2.1 Metric tensor

Intuitively, a metric tells us the "infinitesimal squared distance" that is associated with an "infinitesimal displacement". Thus a metric g, at each and every point of a manifold M, is a symmetric nondegenerate tensor field of type $(0, 2)$ written as

$$g_{\mu\nu} = g_{\nu\mu}. \tag{A.2}$$

The inverse of the metric tensor is defined as

$$(g_{\mu\nu})^{-1} = g^{\mu\nu}. \tag{A.3}$$

Definitions $(A.2)$ and $(A.3)$ are used to raise and lover indices. Sometimes the notation ds^2 is used instead of the metric tensor to convey the flavor of the metric as representing infinitesimal squared distance and can be written as

$$ds^2 = g_{\mu\nu}dx^\mu dx^\nu \tag{A.4}$$

A.2.2 Energy momentum tensor

This is a rank $(2, 0)$ tensor denoted by $T^{\mu\nu}$ defined as a four momentum p^ν flowing in and out of surfaces of constant x^ν. It describes the density and flux of energy and momentum in spacetime and also obeys conservation laws. It is defined in the coordinate basis ∂_μ as

$$\mathbf{T} = T^{\mu\nu}\partial_\mu\partial_\nu.$$

It is symmetric and divergence free that is, $\nabla_\mu T^{\mu\nu} = 0$.

A.2.3 Riemann curvature tensor

With the above tools we can now describe the curvature in an infinitesimal region of a manifold. We can achieve this using the Riemann tensor, which is implicitly defined as

$$(\nabla_\mu\nabla_\nu - \nabla_\nu\nabla_\mu)V^\rho = R^\rho_{\lambda\mu\nu}V^\lambda$$

and hence it can be shown that

$$R^\rho_{\lambda\mu\nu} = \partial_\mu\Gamma^\rho_{\lambda\nu} - \partial_\lambda\Gamma^\rho_{\mu\nu} + \Gamma^\sigma_{\lambda\nu}\Gamma^\rho_{\sigma\mu} - \Gamma^\rho_{\sigma\lambda}\Gamma^\sigma_{\mu\nu}$$

In general, this tensor has 20 independent components and from it we can construct other useful tensors with fewer components as we describe the curvature of spacetime.

A.2.4 Ricci tensor and Ricci scalar

From the Riemann tensor we can obtain the Ricci tensor and scalar which encodes how volume changes in the manifold and describes curvature due to the presence of matter. The Ricci tensor is obtained by taking the trace of the Riemann tensor and is given by

$$R_{\mu\nu} \equiv g^{\lambda\rho} R_{\lambda\mu\rho\sigma} = R^{\lambda}_{\mu\lambda\nu} \tag{A.5}$$

From the Ricci tensor we obtain the Ricci Scalar/Scalar Curvature which is a scalar field. It is obtained by contracting the Ricci tensor and is given by

$$R \equiv g^{\mu\nu} R_{\mu\nu}. \tag{A.6}$$

From these two objects we can then define another very useful tensor, the Einstein tensor, which is a linear combination of the Ricci tensor and the Ricci Scalar. It s given by

$$G_{\mu\nu} = R_{\mu\nu} - \frac{1}{2} g_{\mu\nu} R \tag{A.7}$$

and is divergence free, that is $\nabla_{\mu} G^{\mu\nu} = 0$.

A.2.5 Weyl tensor

As mentioned in the above sections, the Riemann tensor has in general twenty independent components and these can be represented by a combination of the Ricci tensor and the Weyl tensor, $C^{\rho}_{\sigma\mu\nu}$. The ten components represented by the Ricci tensor will be the trace part of the Riemann tensor and and the Weyl tensor, $C^{\rho}_{\sigma\mu\nu}$, representing the other ten components will be the trace-free part of the Riemann tensor and is defined for manifolds whose dimension is $n \geq 3$ by

$$C^{\rho}_{\sigma\mu\nu} = R^{\rho}_{\sigma\mu\nu} - \frac{2}{n-2}\left(g_{\rho[\mu} R_{\nu]\sigma} - g_{\sigma[\mu} R_{\nu]}\rho\right) + \frac{2}{(n-1)(n-2)} g_{\rho[\mu} g_{\nu]\sigma} R \tag{A.8}$$

The components of this tensor describe the components of curvature that are not generated locally and in a sense they describe the "free-gravitational field" and governs the propagation of gravitational waves.

A.2.6 Einstein's Field Equations

• Space and time (≡ **spacetime**) is considered to be a four-dimensional manifold of events where each event can be thought of as a point in space at an instant of time.

We can then relate the metric tensor, the Ricci tensor and the Ricci scalar to the energy momentum tensor mentioned above to give a relation known as the Einstein's Field Equations

$$R_{\mu\nu} - \frac{1}{2}g_{\mu\nu}R + g_{\mu\nu}\lambda = \frac{8\pi G}{c^4}T_{\mu\nu} \tag{A.9}$$

where G is Newton's gravitational constant, λ is the cosmological constant related to the energy density of space and c is the speed of light in a vacuum. These equations describe how matter curves spacetime and how curved spacetime tells matter how to move. As a result any physical spacetime has to be a solution to these equations. In the non-relativistic limit, (A.9) above reduces to the Poisson's equation, which is equivalent to Newton's law of universal gravitation.

A.3 Useful derivations

A.3.1 Deriving the connection

Using the abstract index notation we have

$$\begin{aligned} 0 &= \nabla_a g_{bc} \\ &= \partial_a g_{bc} - \Gamma^d{}_{ab} g_{dc} - \Gamma^d{}_{ac} g_{bd} \\ \Rightarrow \quad \Gamma^c{}_{ab} + \Gamma^b{}_{ac} &= \partial_c g_{bc} \quad \text{.....(i)} \end{aligned}$$

performing index substitution on the above result, we also have

$$a \rightleftharpoons b: \qquad \Gamma^c{}_{ba} + \Gamma^a{}_{bc} = \partial_b g_{ac} \quad \text{.....(ii)}$$

$$b \rightleftharpoons c: \qquad \Gamma^b{}_{ca} + \Gamma^a{}_{cb} = \partial_c g_{ab} \quad \text{.....(iii)}$$

Adding equations (i) and (ii) and then subtracting (iii) using the symmetry property of Γ we have

$$\begin{aligned} 2\Gamma^c{}_{ab} &= \partial_a g_{bc} + \partial_b g_{ac} - \partial_c g_{ab} \\ \Rightarrow \quad \Gamma^c{}_{ab} &= \frac{1}{2}g^{cd}(\partial_a g_{ad} + \partial_b g_{bd} - \partial_d g_{ab}). \end{aligned}$$

A.3.2 The inner product between coordinate vectors

Using our metric ansatz in which $g = (dt - \frac{B}{A}dz)^2 - \frac{1}{A^2}(dz)^2$ it the follows that

$$\begin{aligned} g_{ab}t^a z^b &= g_{ab}(\partial_t)^a(\partial_z)^b \\ &= \Big[(dt)_a(dt)_b - \frac{2B}{A}(dt)_a(dz)_b - \frac{(1-B^2)}{A^2}(dz)_a(dz)_b\Big] \\ &= \Big[(dt)_b - \frac{2B}{A}(dz)_b\Big](\partial_z)^b \\ &= -\frac{2B}{A} \end{aligned}$$

which clearly vanishes if and only if $B = 0$ thereby implying orthogonality.